



This is a repository copy of *The coupling between Ca²⁺ channels and the exocytotic Ca²⁺ sensor at hair cell ribbon synapses varies tonotopically along the mature cochlea.*

White Rose Research Online URL for this paper:
<http://eprints.whiterose.ac.uk/112347/>

Version: Accepted Version

Article:

Johnson, S.L., Olt, J., Cho, S. et al. (2 more authors) (2017) The coupling between Ca²⁺ channels and the exocytotic Ca²⁺ sensor at hair cell ribbon synapses varies tonotopically along the mature cochlea. *Journal of Neuroscience*. 2867-16. ISSN 0270-6474

<https://doi.org/10.1523/JNEUROSCI.2867-16.2017>

Reuse

This article is distributed under the terms of the Creative Commons Attribution (CC BY) licence. This licence allows you to distribute, remix, tweak, and build upon the work, even commercially, as long as you credit the authors for the original work. More information and the full terms of the licence here:
<https://creativecommons.org/licenses/>

Takedown

If you consider content in White Rose Research Online to be in breach of UK law, please notify us by emailing eprints@whiterose.ac.uk including the URL of the record and the reason for the withdrawal request.



eprints@whiterose.ac.uk
<https://eprints.whiterose.ac.uk/>

Research Articles: Cellular/Molecular

The coupling between Ca²⁺ channels and the exocytotic Ca²⁺ sensor at hair cell ribbon synapses varies tonotopically along the mature cochlea

Stuart L. Johnson^{1,*}, Jennifer Olt^{1,*}, Soyoun Cho^{2,3,*}, Henrike von Gersdorff² and Walter Marcotti¹

¹Department of Biomedical Science, University of Sheffield, Sheffield, S10 2TN, UK.

²The Vollum Institute, Oregon Health & Science University, Portland, Oregon 97239, USA.

³Center for Sensory Neuroscience, Boys Town National Research Hospital, Omaha, NE 68131, USA.

DOI: 10.1523/JNEUROSCI.2867-16.2017

Received: 3 September 2016

Revised: 6 January 2017

Accepted: 10 January 2017

Published: 2 February 2017

Author contribution: All authors helped with the collection and analysis of the data. W.M. and H.v.G. conceived and coordinated the study and wrote the paper.

Conflict of Interest: The authors declare that they have no competing financial interest.

*Contributed equally to the work

This work was supported by the Wellcome Trust to WM (102892) and the National Institute of Deafness and other Communication Disorders (NIDCD; DC004274) to HvG. SLJ is a Royal Society University Research Fellow.

Correspondence should be addressed to To whom correspondence should be addressed: Walter Marcotti (w.marcotti@sheffield.ac.uk), Henrike von Gersdorff (vongersd@ohsu.edu)

Cite as: J. Neurosci ; 10.1523/JNEUROSCI.2867-16.2017

Alerts: Sign up at www.jneurosci.org/cgi/alerts to receive customized email alerts when the fully formatted version of this article is published.

This is an open-access article distributed under the terms of the Creative Commons Attribution License Creative Commons Attribution 4.0 International, which permits unrestricted use, distribution and reproduction in any medium provided that the original work is properly attributed.

Accepted manuscripts are peer-reviewed but have not been through the copyediting, formatting, or proofreading process.

Copyright © 2017 Johnson et al.

1
2
3
4
5
6
7
8
9
10
11
12
13
14
15
16
17
18
19
20
21
22
23
24
25
26
27
28
29
30
31
32
33
34
35
36
37
38
39
40
41
42
43
44
45
46
47
48
49
50
51
52
53
54
55
56
57
58
59
60
61
62
63

1 **The coupling between Ca²⁺ channels and the exocytotic Ca²⁺ sensor at hair cell ribbon**
2 **synapses varies tonotopically along the mature cochlea**

3
4
5 Stuart L. Johnson^{1*}, Jennifer Olt^{1*}, Soyoun Cho^{2,3,*}, Henrike von Gersdorff^{2#} and Walter
6 Marcotti^{1#}

7
8 ¹*Department of Biomedical Science, University of Sheffield, Sheffield, S10 2TN, UK.*

9 ²*The Vollum Institute, Oregon Health & Science University, Portland, Oregon 97239, USA.*

10 ³*Center for Sensory Neuroscience, Boys Town National Research Hospital, Omaha, NE*
11 *68131, USA.*

12
13 *Contributed equally to the work

14
15 **#To whom correspondence should be addressed:**

16 Walter Marcotti (w.marcotti@sheffield.ac.uk)

17 Henrike von Gersdorff (vongersd@ohsu.edu)

18
19 **Running title:** Ca²⁺ channel to exocytosis coupling

20
21 8 Figures. Word count: Abstract, 243; Introduction, 647, Discussion, 1653.

22
23 **Author Information:** The authors declare that they have no competing financial interest.

24
25 **Author contribution:** All authors helped with the collection and analysis of the data. W.M.
26 and H.v.G. conceived and coordinated the study and wrote the paper.

27
28 **Acknowledgements:** This work was supported by the Wellcome Trust to WM (102892) and
29 the National Institute of Deafness and other Communication Disorders (NIDCD; DC004274)
30 to HvG. SLJ is a Royal Society University Research Fellow.

31

64
65
66
67
68
69
70
71
72
73
74
75
76
77
78
79
80
81
82
83
84
85
86
87
88
89
90
91
92
93
94
95
96
97
98
99
100
101
102
103
104
105
106
107
108
109
110
111
112
113
114

1 **Abstract**

2 The cochlea processes auditory signals over a wide range of frequencies and intensities.
3 However, the transfer characteristics at hair cell ribbon synapses are still poorly understood at
4 different frequency locations along the cochlea. Using recordings from mature gerbils, we
5 report here a surprisingly strong block of exocytosis by the slow Ca^{2+} buffer EGTA (10 mM)
6 in basal hair cells tuned to high frequencies (~30 kHz). In addition, using recordings from
7 gerbil, mouse and bullfrog auditory organs, we find that the spatial coupling between Ca^{2+}
8 influx and exocytosis changes from nanodomain in low-frequency tuned hair cells (<~2 kHz)
9 to progressively more microdomain in high-frequency cells (>~2 kHz). Hair cell synapses
10 have thus developed remarkable frequency-dependent tuning of exocytosis: accurate low-
11 latency encoding of onset and offset of sound intensity in the cochlea's base and
12 submillisecond encoding of membrane receptor potential fluctuations in the apex for precise
13 phase-locking to sound signals. We also found that synaptic vesicle pool recovery from
14 depletion was sensitive to high concentrations of EGTA, suggesting that intracellular Ca^{2+}
15 buffers play an important role in vesicle recruitment in both low- and high-frequency hair
16 cells. In conclusion, our results indicate that microdomain coupling plays an important role in
17 the exocytosis of high-frequency hair cells, and suggest a novel hypothesis for why these cells
18 are more susceptible to sound-induced damage than low-frequency cells; high-frequency
19 IHCs must have a low Ca^{2+} buffer capacity in order to sustain exocytosis, thus making them
20 more prone to Ca^{2+} -induced cytotoxicity.

21

22 **Significance Statement**

23 In the inner ear, sensory hair cells signal reception of sound. They do this by converting the
24 sound induced movement of their hair bundles present at the top of these cells, into an
25 electrical current. This current depolarizes the hair cell and triggers the calcium-induced

115
116
117 1 release of the neurotransmitter glutamate that activates the postsynaptic auditory fibres. The
118
119 2 speed and precision of this process enables the brain to perceive the vital components of
120
121 3 sound such as frequency and intensity. We show that the coupling strength between calcium
122
123 4 channels and the exocytosis calcium sensor at inner hair cell synapses changes along the
124
125 5 mammalian cochlea such that the timing and/or intensity of sound is encoded with high
126
127 6 precision.

128
129 7

130 131 8 **Introduction**

132
133 9 The sensory neuroepithelium of vertebrate auditory organs is tonotopically organized such
134
135 10 that the characteristic frequency of the hair cells (the sound frequency at which they respond
136
137 11 best) gradually changes with position along the cochlea. Hair cells have developed unique
138
139 12 morphological, molecular and biophysical features that allow them to distinguish a wide
140
141 13 range of sound frequencies and intensities (Fettiplace and Fuchs, 1999) while maintaining
142
143 14 sub-millisecond temporal precision (Matthews and Fuchs, 2010; Heil and Peterson, 2017).
144
145 15 However, the mechanisms by which hair cell ribbon synapses ensure accurate sound encoding
146
147 16 are still largely unknown (Fuchs, 2005; Safieddine et al., 2012). Ribbons are able to tether a
148
149 17 large number of vesicles at the cell's presynaptic active zones, allowing them to facilitate high
150
151 18 rates of sustained neurotransmission (Glowatzki and Fuchs, 2002; Keen and Hudspeth, 2006).
152
153 19 Vesicle fusion at hair cell synapses is triggered by Ca^{2+} entry through $\text{Ca}_v1.3$ Ca^{2+} channels
154
155 20 (Platzer et al., 2000), clustered at the cell's presynaptic active zones (Roberts et al., 1990;
156
157 21 Coggins and Zenisek, 2009; Frank et al., 2010), and uses otoferlin as the major Ca^{2+} sensor
158
159 22 for exocytosis (Roux et al., 2006). However, how Ca^{2+} is able to regulate exocytosis at mature
160
161 23 ribbon synapses is still mostly undetermined.

162
163
164 24 Spatial tightening between Ca^{2+} channels and docked vesicles improves release efficiency
165
166 25 and is important for fast and high-fidelity neurotransmission not only at functionally mature

167
168
169 1 sensory synapses (e.g. calyx of Held: Fedchyshyn and Wang, 2005; Leão and von Gersdorff,
170
171 2 2009; Chen et al., 2015), but also in the squid giant synapse (Augustine et al., 1991) and
172
173 3 mammalian conventional synapses (Bucurenciu et al., 2008; Schmidt et al., 2013). Calcium
174
175 4 nanodomain coupling between a few Ca^{2+} channels and the exocytotic Ca^{2+} sensor (Neher,
176
177 5 1998; Stanley, 2016) has also been proposed to control vesicle fusion in IHCs (Brandt et al.,
178
179 6 2005; Wong et al., 2014). This tight coupling has the advantage of providing accurate
180
181 7 temporal encoding for phase-locking to low-frequency tones (Rose et al., 1967; Li et al.,
182
183 8 2014) and also allows for the synchronized release of multiple vesicles (Graydon et al., 2011),
184
185 9 which produces large AMPA mediated excitatory postsynaptic currents (Glowatzki and
186
187 10 Fuchs, 2002). However, another hypothesis is that the coupling of Ca^{2+} influx and exocytosis
188
189 11 is controlled by the cooperativity of many channels (Ca^{2+} microdomain) and it is the Ca^{2+}
190
191 12 sensor that generates the efficient exocytosis in mature IHC ribbon synapses (Johnson et al.,
192
193 13 2010).

194
195 14 We have previously investigated the effect of the fast Ca^{2+} chelator BATPA on exocytosis
196
197 15 and found it to be comparable in apical and basal gerbil IHCs (Johnson et al., 2008).
198
199 16 However, BAPTA chelates Ca^{2+} independently from the tightness of the coupling between the
200
201 17 Ca^{2+} source and the sensor for vesicle fusion (Wang and Augustine, 2015). Here we used
202
203 18 instead the “slow” Ca^{2+} chelator EGTA, which has similar affinities for Ca^{2+} as BAPTA, but a
204
205 19 140-fold slower ON-binding rate (Naraghi and Neher, 1997), which allows it to bind Ca^{2+}
206
207 20 slower than the sensor for exocytosis and as such act as a high-pass temporal filter for Ca^{2+}
208
209 21 (Wang and Augustine, 2015). Therefore, we investigated the effect of varying the intracellular
210
211 22 EGTA concentration in hair cells positioned at different locations along the mammalian
212
213 23 cochlea (mouse and gerbil) and the amphibian papilla (bullfrog), thus covering cells tuned to
214
215 24 sound frequencies from ~300 Hz to ~30 kHz. We found that the coupling between the Ca^{2+}
216
217 25 channels and the exocytotic Ca^{2+} sensor at hair cell ribbon synapses changes with high-

218
219
220
221
222
223
224
225
226
227
228
229
230
231
232
233
234

1 frequency cells being more microdomain, allowing them to better encode a large dynamic
2 range of sound intensities, whereas low-frequency cells operate via Ca^{2+} nanodomains for
3 precise time encoding. We also found that recovery from vesicle pool depletion was slowed
4 by high EGTA concentrations. We propose that exocytosis at mature hair cell ribbon synapses
5 can operate via either Ca^{2+} nanodomain or microdomain depending on their location along the
6 cochlea, the function of which could be to optimize the responses of these primary auditory
7 receptors.
8

235
236
237
238
239
240
241
242
243
244
245
246
247
248
249
250
251
252
253
254
255
256
257
258
259
260
261
262
263
264
265
266
267
268
269
270
271
272
273
274
275
276
277
278
279
280
281
282
283
284
285

1 **Materials and Methods**

2 *Electrophysiology from mammalian hair cells*

3 IHCs from young adult gerbils of either sex (Müller, 1996) were studied in acutely
4 dissected organs of Corti from postnatal day 18 (P18) to P60, where the day of birth is P0.
5 Recordings were performed from IHCs positioned in the apical, middle and basal gerbil
6 cochlea of overlapping age range, which correspond to the *in vivo* mean characteristic
7 frequency (CF) of ~0.35 kHz, ~2.5 kHz and ~30 kHz, respectively. Experiments were also
8 performed from P19 to P26 mouse (of either sex) IHCs positioned in the apical coil of the
9 cochlea with a mean CF of ~3.0 kHz. All experiments in mice and gerbils were performed in
10 accordance with Home Office regulations under the Animals (Scientific Procedures Act) 1986
11 and following approval by the University of Sheffield Ethical Review Committee.

12 Cochleae were dissected from gerbils and mice in normal extracellular solution (in mM):
13 135 NaCl, 5.8 KCl, 1.3 CaCl₂, 0.9 MgCl₂, 0.7 NaH₂PO₄, 5.6 D-glucose, 10 HEPES-NaOH.
14 Sodium pyruvate (2 mM), amino acids and vitamins were added from concentrates (Fisher
15 Scientific, Loughborough, UK). The pH was adjusted to 7.5 (osmolality ~308 mmol kg⁻¹).
16 The dissected cochlear coils were transferred to a microscope chamber containing
17 extracellular solution and viewed using an upright microscope (Olympus BX51WI or Nikon
18 FN1) with Nomarski DIC optics and a long working distance 60X water-immersion objective.

19 Gerbil and mouse recordings were performed at body temperature (34-37 °C) using an
20 Optopatch amplifier (Cairn Research Ltd, Faversham, UK). Patch pipettes (2-3 MΩ) were
21 coated with surf-wax (Mr Zoggs SexWax, CA, USA) and contained (in mM): 106 Cs-
22 glutamate, 20 CsCl, 3 MgCl₂, 1 EGTA-CsOH, 5 Na₂ATP, 0.3 Na₂GTP, 5 HEPES-CsOH, 10
23 Na₂-phosphocreatine (pH 7.3, 294 mmol kg⁻¹). In the experiments in which 1 mM EGTA was
24 replaced by different EGTA concentrations (0.1, 5, and 10 mM) Cs-glutamate was adjusted to
25 keep the osmolality constant. In a few experiments, perforated patch was used, and the

286
287
288 1 pipette-filling solution contained (in mM): 110 K-aspartate, 21 CsCl, 3 MgCl₂, 5 Na₂ATP, 1
289
290 2 BAPTA, 5 HEPES-CsOH, 10 Na₂-phosphocreatine (pH 7.3; 295 mmol kg⁻¹). The antibiotic
291
292 3 amphotericin B (Merck Millipore, Hertfordshire, UK) was dissolved in dry DMSO before
293
294 4 dilution in the above intracellular solution to 120 or 240 µg ml⁻¹ (Johnson et al., 2007).
295
296 5 Real-time changes in membrane capacitance (ΔC_m) were measured as previously
297
298 6 described (Johnson et al., 2008; 2010). Briefly, a 4 kHz sine wave of 13 mV RMS was
299
300 7 applied to IHCs from -81 mV and was interrupted for the duration of the voltage step. The
301
302 8 sine wave was small enough not to activate any significant membrane current since ΔC_m
303
304 9 requires a high and constant membrane resistance (R_m), which was $738 \pm 61 \text{ M}\Omega$ ($n = 87$). In
305
306 10 the experiments carried out at the physiological membrane potentials (**Fig. 8**), our single sine
307
308 11 wave was sufficiently rapid to activate only a small amount of tonic I_{Ca} , evident by the
309
310 12 comparatively large R_m in these recordings ($639 \pm 77 \text{ M}\Omega$, $n = 20$), which could possibly lead
311
312 13 to some facilitation of vesicle release (Cho et al., 2011). The capacitance signal from the
313
314 14 Optopatch was filtered at 250 Hz and sampled at 5 kHz. ΔC_m was measured by averaging the
315
316 15 C_m trace over a 200 ms period following the voltage step and subtracting the pre-pulse
317
318 16 baseline. Data were acquired using pClamp software (RRID:SCR_011323) and a Digidata
319
320 17 1440A (Molecular Devices, CA, USA) and analysed with Origin 2016 (OriginLab, USA,
321
322 18 RRID:SCR_002815). Membrane potentials were corrected for the voltage drop across the
323
324 19 series resistance (whole-cell recordings: apical coil IHCs, $4.8 \pm 0.1 \text{ M}\Omega$, $n = 60$; middle, $4.9 \pm$
325
326 20 $0.2 \text{ M}\Omega$, $n = 12$; basal, $5.5 \pm 0.2 \text{ M}\Omega$, $n = 45$; perforated patch recordings: apical coil IHCs,
327
328 21 $5.2 \pm 0.2 \text{ M}\Omega$, $n = 4$; basal, $4.8 \pm 0.1 \text{ M}\Omega$, $n = 5$) and a liquid junction potential of -11 mV,
329
330 22 measured between electrode and bath solutions. The cell membrane capacitance (C_m) in
331
332 23 whole-cell was: apical coil IHCs: $11.6 \pm 0.2 \text{ pF}$, $n = 60$; middle: $11.3 \pm 0.5 \text{ pF}$, $n = 12$; basal:
333
334 24 $11.4 \pm 0.4 \text{ pF}$, $n = 45$; C_m in perforated patch was: apical coil IHCs: $10.8 \pm 0.3 \text{ pF}$, $n = 4$;
335
336 25 basal: $10.0 \pm 0.5 \text{ pF}$, $n = 5$. The average voltage-clamp time constant (product of R_s and C_m)

337
338
339 1 in whole-cell was $56 \pm 2 \mu\text{s}$ in apical, $55 \pm 2 \mu\text{s}$ in middle and $62 \pm 4 \mu\text{s}$ in basal IHCs; in
340
341 2 perforated patch it was $55 \pm 2 \mu\text{s}$ in apical and $48 \pm 2 \mu\text{s}$ in basal IHCs. Experiments were
342
343 3 performed in the presence of 30 mM TEA and 15 mM 4-AP (Fluka, Sigma-Aldrich, UK) to
344
345 4 block the BK current ($I_{K,r}$; Kros et al., 1998) and delayed rectifier K^+ currents ($I_{K,neo}$ and $I_{K,s}$),
346
347 5 and linopirdine (80 μM ; Tocris, Bristol, UK) to block $I_{K,n}$ (Marcotti et al., 2003).
348

349 6 Statistical comparisons of means were made by the two-tailed t -test or, for multiple
350
351 7 comparisons, analysis of variance, one-way ANOVA followed by the Bonferroni test. Means
352
353 8 are quoted \pm S.E.M. and $p < 0.05$ indicates statistical significance.
354

355 9

356 357 10 ***Electrophysiology from bullfrog auditory hair cells***

358
359 11 Following an OHSU (IACUC) approved animal care protocol, amphibian papillae of
360
361 12 adult female or male bullfrogs (*Rana catesbeiana*) were carefully dissected as previously
362
363 13 described (Keen and Hudspeth, 2006; Li et al., 2009). Semi-intact preparations of hair cells
364
365 14 and their connecting afferent fibers were placed in a recording chamber with artificial
366
367 15 perilymph containing (in mM): 95 NaCl, 2 KCl, 2 CaCl₂, 1 MgCl₂, 25 NaHCO₃, 3 Glucose, 1
368
369 16 creatine, 1 Na-pyruvate, pH adjusted to 7.3 with NaOH, and continuously bubbled with 95%
370
371 17 O₂ and 5% CO₂ (osmolality 230 mmol kg⁻¹). Oxygenated artificial perilymph was perfused
372
373 18 continuously (2-3 ml/min) during the recordings, which were performed at room temperature.
374

375 19 An Olympus BX51WI microscope equipped with a 60x water-immersion objective lens
376
377 20 (Olympus) and digital CCD camera (QImaging Scientific, Canada) were used to view the
378
379 21 preparation and electrophysiological recordings were performed in the middle area of
380
381 22 amphibian papillae at an average CF of about 0.4 kHz (Li et al., 2014). All recordings were
382
383 23 performed at room temperature using an EPC-10/2 patch-clamp amplifier and Patchmaster
384
385 24 software (HEKA, Germany, RRID:SCR_000034). The control intracellular pipette solution
386
387 25 contained (in mM): 77 Cs-gluconate, 20 CsCl, 1 MgCl₂, 10 TEA-Cl, 10 HEPES, 2 EGTA, 3

388
389
390
391
392
393
394
395
396
397
398
399
400
401
402
403
404
405
406
407
408
409
410
411
412
413
414
415
416
417
418
419
420
421
422
423
424
425
426
427
428
429
430

1 Mg-ATP, 1 Na-GTP and 5 Na₂-phosphocreatine (adjusted to pH 7.3 with CsOH). The amount
2 of Cs-gluconate was adjusted to match osmolarity of 230 mmol kg⁻¹ for pipette solution
3 containing 0.1 mM and 10 mM EGTA instead of 2 mM EGTA. For whole-cell recordings,
4 patch pipettes of borosilicate glass were pulled to resistances of 6 to 7 MΩ for hair cells and 8
5 to 9 MΩ for afferent fibers. Hair cells were voltage-clamped with a resting membrane
6 potential of either -60 mV or -90 mV and afferent fibers were held at -90 mV (Cho and von
7 Gersdorff, 2014). Membrane potentials were corrected for a liquid junction potential of 10
8 mV. The current signal was low-pass filtered at 5.0 kHz and sampled at 100 kHz. The
9 averaged uncompensated series resistances in whole-cell recordings were 12.1 ± 0.2 MΩ for
10 hair cells (*n* = 93) and 26.5 ± 1.7 MΩ for afferent fibres (*n* = 17). The measurements of the
11 whole-cell membrane capacitance (*C_m*) from hair cells were performed under voltage-clamp
12 with the “Sine + DC” method (Lindau and Neher, 1988; Gillis, 2000) using an EPC-10/2
13 (HEKA) patch-clamp amplifier and Patchmaster software (HEKA). Under voltage-clamp
14 conditions, 2 kHz sine waves were superposed on the holding potential and the resulting
15 current response was used to calculate *C_m* via a Patchmaster software emulator of a lock-in
16 amplifier (Gillis, 2000).

17 Data analysis was performed with Igor Pro software (WaveMetrics, OR, USA,
18 RRID:SCR_000325) and Prism (GraphPad Software, RRID:SCR_002798). Statistical
19 significance was assessed with unpaired *t*-test and one-way ANOVA followed by the
20 Bonferroni test. Data are expressed as mean ± S.E.M.

21

431
432
433
434
435
436
437
438
439
440
441
442
443
444
445
446
447
448
449
450
451
452
453
454
455
456
457
458
459
460
461
462
463
464
465
466
467
468
469
470
471
472
473
474
475
476
477
478
479
480
481

1 **Results**

2 Whole-cell patch-clamp recordings were used to investigate Ca^{2+} dependent exocytosis in
3 hair cells at specific characteristic frequencies (CF) of the mature gerbil, mouse and bullfrog
4 auditory organs. Although the mouse and the frog are the most common animal models used
5 for hearing research, they are mainly tuned to high- (mouse hearing frequency range: ~2-100
6 kHz, Ehret, 1975; Greenwood, 1990) and low- (bullfrog amphibian papilla: ~0.15-1.2 kHz,
7 Lewis, et al., 1982; Li et al. 2014) frequency, respectively. The advantage of the gerbil is that
8 it has an extended low-frequency hearing range (~0.1 to 60 kHz, Müller, 1996), more similar
9 to human hearing (~0.02 to 20 kHz: see Greenwood, 1990), which should demarcate better
10 any tonotopic differences along the spiral extension of the cochlea in a single mammalian
11 species.

12 To obtain physiologically relevant data, measurements were performed at body
13 temperature (Johnson et al., 2005; 2010; Nouvian, 2007) and using the extracellular Ca^{2+}
14 concentration present in the perilymph surrounding the IHCs (1.3 mM: Wangemann and
15 Schacht, 1996). The physiological coupling between Ca^{2+} influx and the synaptic machinery
16 was investigated from experiments in which exocytosis was recorded in the presence of
17 different intracellular concentrations of EGTA. This enables increases in intracellular Ca^{2+} to
18 be buffered only relatively far away from its source and thus intercept Ca^{2+} travelling within a
19 microdomain to the Ca^{2+} sensor for exocytosis (Neher, 1998; Stanley, 2016). This is different
20 from the action of the Ca^{2+} chelator BAPTA, which binds Ca^{2+} more rapidly than the Ca^{2+}
21 sensor for exocytosis and as such is able to chelate Ca^{2+} independently of the tightness of the
22 coupling between the Ca^{2+} source and the exocytotic Ca^{2+} sensor (Wang and Augustine,
23 2015). As such, synaptic coupling can be inferred by the different effectiveness of EGTA and
24 BAPTA in decoupling Ca^{2+} channels from the Ca^{2+} sensor for exocytosis. Physiological
25 processes that are prevented by BAPTA but not by EGTA are mediated by a local or

482
483
484
485
486
487
488
489
490
491
492
493
494
495
496
497
498
499
500
501
502
503
504
505
506
507
508
509
510
511
512
513
514
515
516
517
518
519
520
521
522
523
524
525
526
527
528
529
530
531
532

1 nanodomain coupling, while those that are blocked by both imply the presence of a longer
2 distance between the Ca^{2+} source and its sensor (microdomain) (e.g. Adler et al., 1991, Borst
3 and Sakmann, 1996; Meinrenken et al., 2002; Fedchyshyn and Wang, 2005; Wang and
4 Augustine, 2015).

6 **Frequency-dependent variation in the coupling of Ca^{2+} influx and exocytosis**

7 Calcium-dependent exocytosis was measured from IHCs (P20-P27) positioned in the
8 apical (low-frequency: CF \sim 0.35 kHz), middle (CF \sim 2.5 kHz) and basal (high-frequency: CF
9 \sim 30 kHz) regions of the gerbil cochlea. Calcium currents (I_{Ca}) and corresponding ΔC_m
10 recordings from IHCs positioned along the gerbil cochlea are shown in **Fig. 1**. Recordings
11 were obtained in response to 50 ms depolarizing voltage steps (holding potential of -81 mV),
12 which allows the release of only vesicles docked at the active zones, resembling the readily
13 releasable pool (RRP), when performing experiments using physiological 1.3 mM
14 extracellular Ca^{2+} at body temperature (see **Fig. 2** and Johnson et al., 2005; 2010). The size of
15 I_{Ca} was not significantly affected by the different concentrations of EGTA or by the position
16 of the IHC along the cochlea (Apical IHCs: 0.1 mM EGTA -141 ± 9 pA, $n = 6$; 10 mM
17 EGTA -176 ± 18 pA, $n = 8$; Middle IHCs: 0.1 mM EGTA -122 ± 21 pA, $n = 6$; 10 mM
18 EGTA -129 ± 9 pA, $n = 7$; Basal IHCs: 0.1 mM EGTA -136 ± 10 pA, $n = 13$; 10 mM EGTA
19 -139 ± 13 pA, $n = 10$). This is consistent with previous findings showing that the size of I_{Ca} in
20 apical and basal gerbil IHCs was unaffected by different concentrations of the intracellular
21 Ca^{2+} buffer BAPTA (see Fig. 5 in Johnson et al., 2008). In 0.1 mM EGTA, ΔC_m was found to
22 be not significantly different in IHCs along the cochlea ($p = 0.9$, overall one-way ANOVA).
23 While in apical IHCs 10 mM EGTA did not significantly affect ΔC_m (9.6 ± 1.0 fF, $n = 8$)
24 compared to 0.1 mM EGTA (10.5 ± 0.8 fF, $n = 6$, $p = 0.1$) (**Fig. 1 A,D**), the ability of the Ca^{2+}
25 chelator EGTA to uncouple Ca^{2+} influx and exocytosis greatly increased towards the high-

533
534
535 1 frequency region of the gerbil cochlea. In the presence of 0.1 mM intracellular EGTA, the
536
537 2 size of the induced ΔC_m in IHCs from the middle (19.1 ± 2.1 fF, $n = 6$, **Fig. 1B,E**) and basal
538
539 3 (22.7 ± 3.9 fF, $n = 13$, **Fig. 1C,F**) cochlear regions were significantly larger ($p < 0.005$; $p <$
540
541 4 0.0001 , respectively) than the values obtained when EGTA was increased to 10 mM (middle:
542
543 5 8.5 ± 1.5 fF, $n = 7$, **Fig. 1B,E**; basal: 1.3 ± 0.9 fF, $n = 10$, **Fig. 1C,F**). In 10 mM EGTA, ΔC_m
544
545 6 was significantly ($p < 0.001$) smaller in basal and middle IHCs compared to apical cells. With
546
547 7 10 mM intracellular EGTA, the largely reduced or absent ΔC_m in middle and basal IHCs,
548
549 8 respectively, suggests the presence of a microdomain coupling between the Ca^{2+} channels and
550
551 9 the Ca^{2+} sensor for vesicle fusion. This finding is also supported by the fact that while the size
552
553 10 of ΔC_m in apical IHCs (0.1 mM EGTA: **Fig. 1D**) is comparable to that previously reported
554
555 11 using 1 mM intracellular EGTA (50 ms voltage step: Johnson et al., 2008), that measured in
556
557 12 basal IHCs (**Fig. 1F**) was in most cells larger despite the similar number of synaptic ribbons
558
559 13 per cell in the two regions (Johnson et al., 2009; Meyer et al., 2009). Since low frequency
560
561 14 IHCs seem to experience a nanodomain scenario, decreasing the concentration of EGTA from
562
563 15 1 mM (Johnson et al., 2008) to 0.1 mM (**Fig. 1D**) is unlikely to result in a different ΔC_m .
564
565 16 However, the microdomain scenario in high-frequency IHCs would allow Ca^{2+} to travel
566
567 17 further when reducing the concentration of EGTA from 1 mM to 0.1 mM, and most likely
568
569 18 able to recruit a small part of the secondary releasable pool in some IHCs (see below).
570
571 19 In order to investigate whether the vesicle pool dynamics in high EGTA also varied as a
572
573 20 function of frequency position, we measured the rate of neurotransmitter release in gerbil
574
575 21 IHCs (P18-P31) by measuring ΔC_m in response to depolarizing voltage steps to -11 mV of
576
577 22 varying duration (2 ms to 1.0 s: **Fig. 2**; inter-step interval was at least 11 s), which allowed us
578
579 23 to investigate the emptying of different synaptic vesicle pool populations. When using 1 mM
580
581 24 intracellular EGTA and 1.3 mM extracellular Ca^{2+} , stimuli shorter than ~ 50 ms reveal the
582
583 25 RRP (see also Johnson et al., 2005; 2010). Longer steps induce the release of vesicles from a

584
585

586 1 secondarily releasable pool (SRP) that is located further away from the Ca^{2+} channels (frog:
587
588 2 Rutherford and Roberts, 2006; mouse: Moser and Beutner, 2000; gerbil: Johnson et al., 2008).
589
590 3 In 10 mM EGTA, the release from the SRP was almost completely abolished in all IHCs
591
592 4 investigated, irrespective of their cochlear location (apical: **Fig. 2A,D**; middle: **Fig. 2B,E**;
593
594 5 basal: **Fig. 2C,F**), which is also in agreement with previous reports in mice (Moser and
595
596 6 Beutner, 2000) and lower vertebrates (Graydon et al., 2011). However, the release from the
597
598 7 RRP was differentially affected along the gerbil cochlea. In apical low-frequency IHCs (~0.35
599
600 8 kHz, **Fig. 2G**) the size of the isolated RRP in 10 mM EGTA (11.7 ± 1.2 fF, $n = 5$) was not
601
602 9 significantly different from that obtained in 0.1 mM EGTA (18.0 ± 2.3 fF, $n = 8$, $p = 0.07$,
603
604 10 from fits to individual IHCs), as also shown in **Fig. 1A**. The initial release rate was also
605
606 11 similar between the two recording conditions (0.1 mM EGTA: 817 ± 115 fF/s or $22074 \pm$
607
608 12 3109 vesicles/s, $n = 8$; 10 mM EGTA: 596 ± 129 fF/s or 16115 ± 3493 vesicles/s, $n = 5$, $p =$
609
610 13 0.2 , from fits to individual IHCs: **Fig. 2G**). However, compared to 0.1 mM EGTA, 10 mM
611
612 14 EGTA largely reduced the release from the RRP in middle-coil IHCs (middle ~2.5 kHz: 0.1
613
614 15 mM EGTA 20.2 ± 4.6 fF, $n = 5$; 10 mM EGTA 7.1 ± 1.1 fF, $n = 6$, $p < 0.02$, **Fig. 2H**) and
615
616 16 almost completely abolished it in basal cells (basal ~30 kHz: 0.1 mM EGTA 22.1 ± 1.4 fF, n
617
618 17 $= 6$; in 10 mM EGTA the RRP could only be measured in 2 out of 11 IHCs and was 2.4 ± 0.1
619
620 18 fF, **Fig. 2I**). As for IHCs in the apical coil, the initial release rate in middle IHCs was also
621
622 19 similar between the two recording conditions (0.1 mM EGTA: 1000 ± 101 fF/s or $27076 \pm$
623
624 20 2754 vesicles/s, $n = 5$; 10 mM EGTA: 723 ± 141 fF/s or 19558 ± 3708 vesicles/s, $n = 6$, $p =$
625
626 21 0.2 , from fits to individual IHCs).

627
628 22 Using perforated-patch recordings that preserve the endogenous intracellular Ca^{2+}
629
630 23 buffering, we found that the pool sizes and release kinetics of the RRP and SRP were
631
632 24 comparable between apical and basal cells in these physiological conditions (**Fig. 3 A-C**). We
633
634 25 have previously shown that the endogenous buffer concentration was similar between low-

635
636
637 1 and high-frequency gerbil IHCs when expressed as an equivalent BAPTA concentration
638
639 2 (Johnson et al., 2008). However, when the ΔC_m values obtained in perforated patch were
640
641 3 extrapolated to those obtained using different concentrations of EGTA (**Fig. 3 D**), they
642
643 4 revealed a higher sensitivity to Ca^{2+} buffering in high-frequency IHCs (~ 2.9 mM) compared
644
645 5 to low-frequency cells (~ 6.6 mM) (**Fig. 3 D**). However, this is not an indication of the
646
647 6 endogenous buffer in IHCs but provides further evidence for a different exocytotic Ca^{2+}
648
649 7 coupling of the RRP between apical and basal cells.

650
651 8

652 653 9 **Calcium channel and vesicle coupling in high frequency mouse IHCs**

654
655 10 In order to confirm that the different coupling between Ca^{2+} influx and exocytosis
656
657 11 observed in IHCs along the gerbil cochlea (**Figs. 1-3**) was due to the synaptic machinery
658
659 12 being specialised to detect different frequencies, we performed experiments in the mouse and
660
661 13 the bullfrog. **Figure 4A, B** shows the maximal I_{Ca} and the corresponding ΔC_m recorded from
662
663 14 apical IHCs of the mouse cochlea (~ 3.0 kHz) in the presence of either low (0.1 and 1 mM) or
664
665 15 high (5 mM and 10 mM) concentrations of intracellular EGTA, respectively. Note that the
666
667 16 apical coil of the mouse cochlea has a CF in the same range to that of the middle region of the
668
669 17 gerbil cochlea (~ 2.5 kHz: see **Figs. 1 and 2**). The data from 0.1 mM and 1 mM EGTA (**Fig.**
670
671 18 **4**) were pooled together because they produced overlapping results. Responses were obtained
672
673 19 using 50 ms depolarizing voltage steps (10 mV nominal increments) from -81 mV. The
674
675 20 maximal size of I_{Ca} recorded in IHCs (P15-P26) was not significantly different between low
676
677 21 (0.1 and 1 mM: -179 ± 21 pA, $n = 5$, **Fig. 4C**) and high EGTA (5 mM: -115 ± 7 pA, $n = 3$ or
678
679 22 10 mM: -139 ± 11 pA, $n = 5$; **Fig. 4D**). However, the induced ΔC_m was significantly reduced
680
681 23 (overall: $p < 0.002$, one-way ANOVA) in the presence of 5 mM (6.4 ± 0.8 fF, $n = 3$, $p < 0.05$
682
683 24 post-test) or 10 mM EGTA (2.0 ± 1 fF, $n = 5$, $p < 0.01$ post-test) (**Fig. 4D**), compared to the
684
685 25 lower concentrations (0.1 & 1 mM EGTA: 16 ± 3 fF, $n = 6$, **Fig. 4C**).

686
687
688
689
690
691
692
693
694
695
696
697
698
699
700
701
702
703
704
705
706
707
708
709
710
711
712
713
714
715
716
717
718
719
720
721
722
723
724
725
726
727
728
729
730
731
732
733
734
735
736

1 The rate of neurotransmitter release in mouse IHCs (P19-P26) was studied by measuring
2 ΔC_m in response to depolarizing voltage steps of increasing duration as described for **Fig. 2**.
3 Voltage steps of up to about 50 ms (RRP) produced an increase in ΔC_m that could be
4 approximated with a single exponential (**Fig. 4F**). However, in the presence of 5 mM or 10
5 mM intracellular EGTA the largely reduced size of the RRP (as shown in **Fig. 4A,B**) was also
6 associated with a significantly reduced initial release rate (5 mM: 374 ± 33 fF/s or $10112 \pm$
7 877 vesicles/s, $n = 4$, $p < 0.05$ post-test; 10 mM 203 ± 36 fF/s or 5500 ± 976 vesicles/s, $n = 3$,
8 $p < 0.01$ post-test) compared to that measured in lower EGTA concentrations (614 ± 75 fF/s
9 or 16589 ± 2036 vesicles/s, $n = 5$: average from fit to single cells; overall: $p < 0.005$, one-way
10 ANOVA) (**Fig. 4F**). The SRP in high EGTA was almost absent (**Fig. 4E**). Considering that
11 the total number of ribbons per IHC is about twenty (Brandt et al., 2005; Mayer et al., 2009;
12 Zampini et al., 2010), the vesicle release rate per ribbon was about 829 vesicles/s (low EGTA)
13 506 vesicles/s (5 mM EGTA) and 275 vesicles/s (10 mM EGTA) vesicles/s. This reduced
14 exocytosis in mouse IHCs in the presence of high concentrations of EGTA has previously
15 been reported in young (P12-P14: Vincent et al., 2014) but not in more mature (>P14: Moser
16 and Beutner, 2000) cells using unphysiologically high extracellular Ca^{2+} (5-10 mM) and room
17 temperature.

18

19 **Calcium channel and vesicle coupling in low frequency tuned bullfrog hair cells**

20 We next investigated I_{Ca} and the corresponding ΔC_m in single hair cells from a semi-intact
21 adult bullfrog amphibian papilla preparation, which are tuned to a lower frequency range
22 (~400-500 Hz; Li et al., 2014), to examine the exocytotic Ca^{2+} coupling. To measure I_{Ca} and
23 ΔC_m , we stimulated the hair cells with voltage-clamp step depolarizations from -90 mV to
24 -30 mV for various durations (**Fig. 5A**). A depolarization to -30 mV elicits the peak I_{Ca} in
25 bullfrog hair cells (Graydon et al., 2011). As the pulse duration increased so did the resulting

737
738
739
740
741
742
743
744
745
746
747
748
749
750
751
752
753
754
755
756
757
758
759
760
761
762
763
764
765
766
767
768
769
770
771
772
773
774
775
776
777
778
779
780
781
782
783
784
785
786
787

1 ΔC_m (**Fig. 5A**; see also Li et al., 2009). We compared ΔC_m in response to depolarizing pulses
2 with 2 mM and 10 mM intracellular EGTA (**Fig. 5A and B**). Depolarizing pulses shorter than
3 50 ms did not show any significant difference in ΔC_m between 2 mM and 10 mM EGTA
4 (unpaired t-test, $P < 0.05$; see also Graydon et al., 2011). However, ΔC_m was significantly
5 larger for 50 ms pulses (**Fig. 5B**). Our previous study shows that a pulse shorter than 50 ms
6 from -90 mV to -30 mV only triggers the RRP of hair cells, which includes about 700
7 vesicles per hair cell, or 12 vesicles per synaptic ribbon (Graydon et al., 2011). To confirm
8 this insensitivity of the RRP to EGTA, we compared ΔC_m in response to pulses of 20 ms and
9 500 ms with 0.1 mM, 2 mM and 10 mM intracellular EGTA (**Fig. 5C,D**). The average ΔC_m in
10 response to a 20 ms pulse was not significantly different with 0.1 mM (21.7 ± 1.7 fF, $n = 21$),
11 2 mM (17.8 ± 1.4 fF, $n = 18$), and 10 mM EGTA (17.4 ± 1.0 fF, $n = 14$, one-way ANOVA,
12 **Fig. 5C**). In contrast, different concentrations of intracellular EGTA significantly changed the
13 average ΔC_m in response to a 500 ms pulse (overall: $p < 0.006$, one-way ANOVA, **Fig. 5D**):
14 ΔC_m with 0.1 mM (203.8 ± 34.8 fF, $n = 16$) which was significantly different from that with
15 10 mM EGTA (104.1 ± 8.5 fF, $n = 13$, $p < 0.05$, post-test; **Fig. 5A**), although the ΔC_m with 2
16 mM (147.3 ± 9.1 fF, $n = 34$) was not significantly different from those with 0.1 mM and 10
17 mM EGTA (post-test). In summary, our data suggests that, in stark contrast to mouse high-
18 frequency IHCs (**Fig. 4**), the release of vesicles in the RRP from low-frequency hair cells is
19 relatively insensitive to the concentration of intracellular EGTA. However, for longer
20 depolarizing pulses of 50 ms and 500 ms we do find that release is significantly reduced by 10
21 mM EGTA. This suggests that during a longer depolarizing pulse the recruitment of vesicles
22 from a reserve pool is sensitive to global rises in intracellular free Ca^{2+} and is thus sensitive to
23 the intracellular levels of EGTA. The RRP of amphibian papilla hair cells, which are tuned to
24 low frequency sound signals, is thus controlled by nanodomain Ca^{2+} coupling.

788
789
790
791
792
793
794
795
796
797
798
799
800
801
802
803
804
805
806
807
808
809
810
811
812
813
814
815
816
817
818
819
820
821
822
823
824
825
826
827
828
829
830
831
832
833
834
835
836
837

1 Paired-pulse responses in gerbil IHCs and bullfrog auditory hair cells

2 We investigated possible differences in the rate of ΔC_m recovery from gerbil IHCs (P18-
3 P27) positioned in the apical and basal cochlear regions by applying a two-pulse protocol in
4 which cells were depolarized to -11 mV for 50 ms, which recruited the RRP, while changing
5 the interpulse interval (IPI) from 10 ms up to 1.0 s (**Fig. 6A**). Examples of ΔC_m recorded from
6 apical and basal IHCs using the two-pulse protocol and in the presence of either 0.1 mM
7 EGTA or 10 mM EGTA are shown in **Fig. 6B,C**, respectively. The average ΔC_m ratio
8 ($\Delta C_m^2/\Delta C_m^1$; see **Fig. 6A**) from apical IHCs (0.1 mM EGTA, $n = 12$; 10 mM EGTA, $n = 6$)
9 was plotted against IPI and the data were well approximated with a single exponential
10 function (**Fig. 6D**). For basal IHCs the average ΔC_m ratio in 0.1 mM EGTA showed an initial
11 depression at short intervals and then facilitation at around 100 ms (**Fig. 6E**; see also
12 Goutman and Glowatzki, 2011; Cho et al., 2011).

13 To study whether the concentration of EGTA can affect short-term plasticity at low-
14 frequency tuned hair cell synapses (tuned to ~ 400 -500 Hz), we performed paired recordings
15 between adult bullfrog hair cells and their afferent fibres. We held presynaptic hair cells at
16 -60 mV, which is close to their physiological *in vivo* resting membrane potential (Crawford
17 and Fettplice, 1980; Pitchford and Ashmore, 1987) and measured paired-pulse ratios of
18 EPSCs using 2 mM and 10 mM intracellular EGTA in the patch pipette of the hair cell (**Fig.**
19 **7A**). Hair cells were stimulated by a pair of 20 ms depolarizing pulses from -60 mV to -30
20 mV with various interpulse intervals and EPSCs were recorded from the connected
21 postsynaptic afferent fibres (**Fig. 7A,B**). The average amplitude of the first EPSC was not
22 significantly different with 2 mM (2504 ± 307 pA, $n = 20$) and 10 mM EGTA (2582 ± 499
23 pA, $n = 18$, $p = 0.89$, unpaired *t*-test), showing that the RRP exocytosis released by 20 ms
24 pulses is insensitive to the concentration of EGTA. These results using AMPA receptor

838
839
840
841
842
843
844
845
846
847
848
849
850
851
852
853
854
855
856
857
858
859
860
861
862
863
864
865
866
867
868
869
870
871
872
873
874
875
876
877
878
879
880
881
882
883
884
885
886
887
888

1 mediated EPSCs confirm our earlier results with ΔC_m changes in hair cells held at -90 mV
2 (see **Fig. 5A,C**).

3 We next studied the changes in paired-pulse ratio under 2 mM and 10 mM EGTA. While
4 hair cells were held at -60 mV, the second EPSC was smaller than the first EPSC throughout
5 various interpulse intervals (from 3 ms to 4 s), showing a robust paired-pulse depression (**Fig.**
6 **7A,B**). For short interpulse intervals such as 20 ms, this synapse shows very strong paired-
7 pulse depression and as the interpulse intervals get longer, paired-pulse depression recovers
8 (**Fig. 7A,B**). This depression is not caused by AMPA receptor desensitization (Graydon et al.,
9 2014), and more likely reflects vesicle pool depletion (Cho et al., 2011). We examined
10 whether the enhanced level of EGTA can affect the recovery from paired-pulse depression.
11 The paired-pulse ratio (PPR) was calculated by the ratio of EPSC amplitudes ($EPSC_2/EPSC_1$).
12 With 2 mM intracellular EGTA, a double exponential function can fit the recovery of PPR
13 with fast ($\tau_1 = 15$ ms; 63 %) and slow ($\tau_2 = 602$ ms; 37 %) time constants (**Fig. 7C**; see also
14 Cho et al., 2011). When we increased the concentration of intracellular EGTA to 10 mM,
15 recovery of paired-pulse depression was delayed for both the fast ($\tau_1 = 92$ ms; 35%) and slow
16 ($\tau_2 = 1161$ ms; 65%) time constants. The median (weighted-mean) time constant increased
17 significantly from 232 ms with 2 mM EGTA to 787 ms with 10 mM EGTA. These data thus
18 indicate that recovery of paired-pulse depression is dependent on global intracellular Ca^{2+}
19 levels within hair cells. This suggests again that the recruitment of vesicles from a reserve
20 vesicle pool to the RRP is sensitive to the intracellular levels of EGTA and, thus to the
21 intracellular free Ca^{2+} .

23 **Exocytosis under physiological resting membrane potential in gerbil IHCs**

24 The above experiments in mice and gerbils were performed using a resting holding
25 potential of -81 mV, which is commonly used for exocytosis (capacitance measurements)

889
890
891
892
893
894
895
896
897
898
899
900
901
902
903
904
905
906
907
908
909
910
911
912
913
914
915
916
917
918
919
920
921
922
923
924
925
926
927
928
929
930
931

1 studies from hair cell ribbon synapses (mouse: Moser and Beutner, 2000; Johnson et al.,
2 2010; Wong et al., 2014; gerbil: Johnson et al., 2009; bullfrog: Li et al., 2009; Cho et al.,
3 2011). Since the estimated *in vivo* resting potential is likely to be around -50 mV for apical
4 and -60 mV for basal IHCs (Johnson et al., 2011; Johnson, 2015), and I_{Ca} has been shown to
5 activate at around -60 mV (gerbils, Johnson et al., 2008), cells will be subjected to some
6 continuous Ca^{2+} influx even at rest (see Materials and Methods). Therefore, we investigated
7 gerbil IHC (P19-P28) exocytosis and the coupling between Ca^{2+} influx and the RRP using the
8 more physiological resting membrane potentials (**Fig. 8**). For these experiments, 1 mM EGTA
9 was used as the intracellular Ca^{2+} buffer in apical and basal IHCs since it produces
10 comparable ΔC_m (Johnson et al., 2008) as those measured in perforated patch recordings (**Fig.**
11 **8E**) for both the RRP and SRP. This also allowed us to test the specific effect of the
12 theoretical *in vivo* membrane potential on the release and replenishment of the RRP. Despite
13 the different resting membrane potentials, the maximal I_{Ca} (apical: -128 ± 13 pA, $n = 7$; basal:
14 -125 ± 11 pA, $n = 9$) and the corresponding ΔC_m (apical: 10.5 ± 1.1 fF; basal: 8.8 ± 1.4 fF)
15 was similar between apical and basal IHCs (**Fig. 8A-D**), as well as the size of the RRP (**Fig.**
16 **8E**). However, the rate of ΔC_m recovery during paired pulses was significantly faster in basal
17 ($\tau = 27 \pm 11$ ms, $n = 6$, from fits to single IHCs, $p < 0.02$) than in apical IHCs ($\tau = 156 \pm 43$
18 ms, $n = 5$). This is in line with our findings in the bullfrog showing that faster recovery
19 depends on the availability of global free intracellular Ca^{2+} present in a microdomain situation
20 (**Fig. 7C**).
21

932
933
934
935
936
937
938
939
940
941
942
943
944
945
946
947
948
949
950
951
952
953
954
955
956
957
958
959
960
961
962
963
964
965
966
967
968
969
970
971
972
973
974
975
976
977
978
979
980
981
982

1 **Discussion**

2 Using physiological recording conditions, in terms of extracellular Ca^{2+} level and body
3 temperature, we show that the coupling between Ca^{2+} channels and the Ca^{2+} -sensor for vesicle
4 fusion changes as a function of the cell's frequency position. While low-frequency hair cells
5 ($< \sim 2$ kHz), which phase-lock to sound, exhibit a nanodomain coupling between Ca^{2+} channels
6 and Ca^{2+} sensor, high-frequency cells have a looser coupling, which becomes progressively
7 more microdomain along the gerbil cochlea. We have also shown that the level of intracellular
8 Ca^{2+} buffer affects the speed of recovery from paired-pulse depression. We propose that either
9 nanodomain or microdomain coupling is present in mature auditory hair cells, the function of
10 which is to preserve the precise temporal coding of sound in phase-locked low-frequency hair
11 cells and stimulus intensity in high-frequency cells, respectively.

12

13 **Mechanisms of Ca^{2+} influx-secretion coupling in IHCs**

14 A characteristic feature of the coupling between Ca^{2+} entry and vesicle fusion at IHC
15 ribbon synapses is the change in the Ca^{2+} dependence of exocytosis from a high-order relation
16 in immature cells to linear in mature post-hearing cells (Brandt et al., 2005; Johnson et al.,
17 2005; 2008; 2010; Wong et al., 2014). However, such linearization in synaptic function only
18 occurs in mature high-frequency IHCs responding to sound frequencies above a few kHz
19 (Johnson et al., 2008; 2009), which encompasses the entire frequency range in the mouse
20 cochlea (~ 3 -100 kHz: Greenwood, 1990) but only the middle and basal regions in the gerbil
21 (~ 0.1 -60 kHz: Müller, 1996). This exocytotic linearization implies that vesicle fusion scales
22 linearly with Ca^{2+} entry, which in mature high-frequency IHCs has been proposed to depend
23 upon the developmental tightening of the spatial coupling between Ca^{2+} channels and release
24 Ca^{2+} sensors (Ca^{2+} -nanodomain coupling: Brandt et al., 2005; Wong et al., 2014). In this
25 scenario, one or very few Ca^{2+} channels are sufficient to govern the release of a nearby vesicle

983
984
985 1 (Brandt et al., 2005; Zampini et al., 2013; Graydon et al., 2011). However, an alternative
986
987 2 hypothesis is that the linearization is due to developmental changes in the Ca^{2+} sensor(s) that
988
989 3 affect the intrinsic Ca^{2+} dependence of the synaptic machinery. Although otoferlin is the
990
991 4 major Ca^{2+} sensor in IHCs (Roux et al., 2006; Safieddine et al., 2012), synaptotagmin IV is
992
993 5 essential for establishing the linear exocytotic Ca^{2+} dependence (Johnson et al., 2010), which
994
995 6 could arise from its inability to bind Ca^{2+} in the C2A domain (Südhof, 2002). In this second
996
997 7 hypothesis, a Ca^{2+} -microdomain coupling scenario could be postulated (Wang and Augustine,
998
999 8 2015). These two synaptic scenarios (i.e. nano- and micro-domain coupling) may in fact co-
000
001 9 exist within the same auditory organ, since low- and high-frequency IHCs are specialized to
002
003 10 emphasize mainly the phasic or sustained components of the cell's *in vivo* receptor potential,
004
005 11 respectively (Johnson, 2015).

006
007 12
008

009 13 **Nano- versus micro-domain coupling at hair cell ribbon synapses**

010
011 14 In squid giant synapses and mature calyx of Held synapses vesicle release is reduced more
012
013 15 effectively by BAPTA than by EGTA (Augustine et al., 1991; Fedchyshyn and Wang, 2005;
014
015 16 Chen et al., 2015; Nakamura et al., 2015), indicating a nanodomain coupling between Ca^{2+}
016
017 17 channels and exocytotic Ca^{2+} sensors at mature synapses. However, recent findings have
018
019 18 shown that mature hippocampal synapses can also operate via a loose coupling (Vyleta and
020
021 19 Jonas, 2014), challenging the view that Ca^{2+} -microdomain mode of Ca^{2+} signalling is only a
022
023 20 characteristic of immature synapses (e.g. Meinrenken et al., 2002; Fedchyshyn and Wang,
024
025 21 2005; Leão and von Gersdorff, 2009; Wang and Augustine, 2015). Instead it suggests that the
026
027 22 vesicle release modality is optimized for specific functional requirements independent from
028
029 23 the stage of cell maturation.

030
031 24 Here we found that the RRP of low frequency hair cell ribbon synapses, in both the
032
033 25 mammalian cochlea (~350 Hz) and bull frog papilla (<1 kHz), were relatively insensitive to

034
035
036 1 EGTA, whereas RRP release from IHCs responding above a few kHz was either largely
037
038 2 reduced (~2-3 kHz) or abolished (~30 kHz). This indicates that the spatial coupling between
039
040 3 Ca^{2+} influx and exocytosis progressively changes along the gerbil auditory organ in order to
041
042 4 cover a wider hearing range (~0.1-60 kHz). Although it has previously been reported that the
043
044 5 RRP in mouse IHCs was insensitive to 5 mM EGTA (Moser and Beutner, 2000), perhaps due
045
046 6 to the use of high unphysiological extracellular Ca^{2+} , paired recordings from IHCs and
047
048 7 auditory afferent fibres in the rat cochlea have demonstrated that the onset and rise time of the
049
050 8 EPSC was largely slowed by 10 mM EGTA (Goutman and Glowatzki, 2007).

051
052 9

053 054 10 **Vesicle recruitment and the Ca^{2+} -dependence of recovery from depression**

055
056 11 We found that apical IHCs tuned to ~350 Hz in the gerbil recovered fully from paired-
057
058 12 pulse depression within ~200 ms for 50 ms depolarizing pulses and with 0.1 mM EGTA. This
059
060 13 recovery rate was slowed by 10 mM EGTA. Similar results were obtained in bullfrog hair
061
062 14 cells tuned to lower CF (400-500 Hz; **Fig. 7C**). The enhanced fast recovery of EPSCs with
063
064 15 lower Ca^{2+} buffering may be due to the greater spread of Ca^{2+} that speeds the replenishment
065
066 16 of vesicles to the ribbon (Van Hook et al., 2014). Recovery from paired-pulse depression was
067
068 17 even faster in basal gerbil IHCs (<100 ms), which is consistent with their microdomain
069
070 18 coupling. These recovery rates are extremely rapid when compared to that in retinal bipolar
071
072 19 cells, which also operate via ribbon synapses (Palmer et al., 2003). This rapid recovery may
073
074 20 be an evolutionary adaptation for hair cell ribbon synapses, which are specialised to detect
075
076 21 rapid sound signals with short gaps and encode these as firing patterns in the auditory nerve.

077
078 22
079

080 23 **Ca^{2+} influx-secretion coupling and hair cell receptor potential**

081
082 24 The receptor potential of low-frequency IHCs (up to a few kHz) has a predominantly
083
084 25 phasic component that is phase-locked to the sound frequency and graded in size to the

085
086
087 1 stimulation intensity (Dallos, 1985; Cheatham and Dallos, 1993). The localisation of low
088
089 2 frequency sound is accomplished by cells in the auditory brainstem that detect minute time
090
091 3 delays in the arrival of the phase-locked afferent activity originating from the two ears (~10
092
093 4 μ s; Grothe et al., 2010). Such a precise temporal coding has to be preserved at IHC ribbon
094
095 5 synapses and the nanodomain coupling scenario would guarantee rapid and reliable vesicle
096
097 6 fusion (Neher, 1998). In the low-frequency cochlear region, a nanodomain coupling would
098
099 7 also be required to explain why the time delay in vesicle fusion is similar at all levels of IHC
100
101 8 depolarization (i.e. stimulus intensity). This property is crucial for the accurate preservation of
102
103 9 stimulus timing at all sound intensities and has been suggested to be governed by the single
104
105 10 Ca^{2+} channel properties of first latency and current amplitude (Magistretti et al., 2015). At
106
107 11 very low frequencies, the relatively slow depolarizing cycle will allow sufficient Ca^{2+} influx
108
109 12 to saturate the exocytotic Ca^{2+} sensor even at low sound intensities. At higher frequencies (up
110
111 13 to ~2 kHz), but still within the limit for phase-locking, the reduced time for Ca^{2+} influx into
112
113 14 IHCs is likely to be insufficient to trigger exocytosis; this could be overcome, in a
114
115 15 nanodomain scenario, by the elementary Ca^{2+} tail currents, where the amplitude and speed of
116
117 16 the current is maximized and constant. Indeed, when sinusoidal stimuli of a few hundred Hz
118
119 17 were applied to rat IHCs or hair cells from the bullfrog papilla, afferent fibres responded with
120
121 18 large EPSCs that occurred more frequently during the repolarizing phase of the cycles
122
123 19 (Goutman, 2012; Li et al., 2014), which corresponded to the Ca^{2+} tail currents.

124
125 20 The filtering characteristics of the hair cell membrane prevents phase-locking above ~2-3
126
127 21 kHz (Palmer and Russell, 1986), so receptor potentials are mainly graded and sustained to
128
129 22 represent sound intensity and stimulus envelope (Russell and Sellick, 1978). High frequency
130
131 23 sound localization is performed by cells that compare inter-aural level differences originating
132
133 24 from graded responses in >3 kHz IHCs of each ear (Caird and Klinke, 1983). Therefore, high-
134
135 25 frequency IHCs are not designed to follow the frequency components of sound, and as such

136
137
138
139
140
141
142
143
144
145
146
147
148
149
150
151
152
153
154
155
156
157
158
159
160
161
162
163
164
165
166
167
168
169
170
171
172
173
174
175
176
177
178
179
180
181
182
183
184
185
186

1 do not require the precise timing provided by nanodomain coupling, which is likely to be
2 unsuitable for accurate intensity coding. Instead, the changes in the amplitude and kinetic
3 properties of the macroscopic I_{Ca} with sound intensity are now more relevant (Magistretti et
4 al., 2015), which is more in line with a microdomain coupling reported in this study.

5 6 **Damage due to loud sounds: why are basal IHCs more susceptible?**

7 We found that high-frequency IHCs (especially those at ~30 kHz) exhibit a strong block of
8 exocytosis by 10 mM EGTA, indicating that these cells cannot have a large endogenous Ca^{2+}
9 buffering capacity, because it would severely impair transmitter release. This was confirmed
10 by the estimated intracellular Ca^{2+} buffer expressed as an equivalent of EGTA concentration
11 (**Fig. 3**). Indeed, a triple knock-out mouse for different Ca^{2+} -binding proteins did not reveal
12 changes in synaptic sound encoding (Pangršič et al., 2015), suggesting that high-frequency
13 IHCs may thus have a relatively low concentration of Ca^{2+} binding proteins. By contrast, low-
14 frequency tuned bullfrog hair cells have an estimated 8 mM of high-affinity Ca^{2+} -binding sites
15 on small mobile proteins (e.g. parvalbumin and calbindin; Heller et al., 2002), suggesting that
16 their endogenous Ca^{2+} buffering capacity may be more equivalent to 10 mM EGTA.

17 High-frequency hair cell synapses are also particularly vulnerable to damage during loud
18 noises and aging, which has been shown to lead to the loss of both IHC synaptic ribbons
19 (Kujawa and Liberman, 2009; Kujawa and Liberman, 2015) and low-spontaneous rate
20 afferent fibers (Furman et al., 2013). We thus propose that low-frequency IHCs may express
21 higher concentrations of Ca^{2+} binding proteins, which will not block exocytosis, but may
22 confer neuroprotection against excessive Ca^{2+} influx during prolonged stimulation. By
23 contrast, the low Ca^{2+} buffer capacity in high-frequency basal IHCs, which is required for
24 their graded release, will make them more prone to Ca^{2+} -induced cytotoxicity. A tonotopic
25 gradient in Ca^{2+} binding protein expression has been reported in auditory hair cells (Patel et

1187
1188

1189 1 al., 2012; Hackney et al., 2003; 2005), which may facilitate a frequency-dependent tuning of
1190

1191 2 exocytosis in some animal species (Rutherford and Roberts, 2006; Patel et al., 2012; Schnee
1192

1193 3 et al., 2005).

1194

1195 4

196
197
198
199
200
201
202
203
204
205
206
207
208
209
210
211
212
213
214
215
216
217
218
219
220
221
222
223
224
225
226
227
228
229
230
231
232
233
234
235
236
237
238
239
240
241
242
243
244
245
246
247
248
249
250
251
252
253
254
255
256
257
258
259
260
261
262

- 1 **References**
- 2 Adler EM, Augustine GJ, Duffy SN, Charlton MP (1991) Alien intracellular calcium
- 3 chelators attenuate neurotransmitter release at the squid giant synapse. *J Neurosci* 11:
- 4 1496-1507.
- 5 Augustine GJ, Adler EM, Charlton MP (1991) The calcium signal for transmitter secretion
- 6 from presynaptic nerve terminals. *Ann N Y Acad Sci* 635: 365-381.
- 7 Brandt A, Khimich D, Moser T (2005) Few $Ca_v1.3$ channels regulate the exocytosis of a
- 8 synaptic vesicle at the hair cell ribbon synapse. *J Neurosci* 25: 11577-11585.
- 9 Beutner D, Voets T, Neher E, Moser T (2001) Calcium dependence of exocytosis and
- 10 endocytosis at the cochlear inner hair cell afferent synapse. *Neuron* 29: 681-690.
- 11 Borst JG, Sakmann B (1996) Calcium influx and transmitter release in a fast CNS synapse.
- 12 *Nature* 383: 431-434.
- 13 Bucurenciu I, Kulik A, Schwaller B, Frotscher M, Jonas P (2008) Nanodomain coupling
- 14 between Ca^{2+} channels and Ca^{2+} sensors promotes fast and efficient transmitter release
- 15 at a cortical GABAergic synapse. *Neuron* 57: 536-545.
- 16 Caird D, Klinke R (1983) Processing of binaural stimuli by cat superior olivary complex
- 17 neurons. *Exp Brain Res* 52: 385-399.
- 18 Cheatham MA, Dallos P (1993) Longitudinal comparisons of IHC ac and dc receptor
- 19 potentials recorded from the guinea pig cochlea. *Hear Res* 68: 107-114.
- 20 Chen Z, Das B, Nakamura Y, DiGregorio DA, Young SM Jr (2015) Ca^{2+} channel to synaptic
- 21 vesicle distance accounts for the readily releasable pool kinetics at a functionally mature
- 22 auditory synapse. *J Neurosci* 35: 2083-2100.
- 23 Cho S, Li GL, von Gersdorff H (2011) Recovery from short-term depression and facilitation
- 24 is ultrafast and Ca^{2+} dependent at auditory hair cell synapses. *J Neurosci* 31: 5682-5692.
- 25 Cho S, von Gersdorff H (2014) Proton-mediated block of Ca^{2+} channels during multivesicular
- 26 release regulates short-term plasticity at an auditory hair cell synapse. *J Neurosci* 34:
- 27 15877-15887
- 28 Coggins M, Zenisek D (2009) Evidence that exocytosis is driven by calcium entry through
- 29 multiple calcium channels in goldfish retinal bipolar cells. *J Neurophysiol* 101: 2601-
- 30 2619.
- 31 Crawford AC, Fettiplace R (1980) The frequency selectivity of auditory nerve fibres and hair
- 32 cells in the cochlea of the turtle. *J Physiol* 306: 79-125.
- 33 Dallos P (1985) Response characteristics of mammalian cochlear hair cells. *J Neurosci* 5:

- 263
264
265 1 1591-1608.
266
267 2 Ehret G (1975) Masked auditory thresholds, critical ratios, and scales of the basilar membrane
268 of the housemouse (*Mus musculus*). *J Comp Physiol* 103: 329–341.
269 3
270
271 4 Fedchyshyn MJ, Wang LY (2005) Developmental transformation of the release modality at
272 the calyx of Held synapse. *J Neurosci* 25: 4131-4140.
273 5
274
275 6 Fettiplace R, Fuchs PA (1999) Mechanisms of hair cell tuning. *Ann Rev Physiol* 61: 809-834.
276
277 7 Frank T, Rutherford MA, Strenzke N, Neef A, Pangršič T, Khimich D, Fejtova A,
278 Gundelfinger ED, Liberman MC, Harke B, Bryan KE, Lee A, Egnér A, Riedel D,
279 Moser T (2010) Bassoon and the synaptic ribbon organize Ca^{2+} channels and vesicles to
280 add release sites and promote refilling *Neuron* 68: 724-738.
281 9
282
283 10 Fuchs PA (2005) Time and intensity coding at the hair cell's ribbon synapse. *J Physiol* 566: 7-
284 12.
285 11
286
287 12
288
289 13 Furman AC, Kujawa SG, Liberman MC (2013) Noise-induced cochlear neuropathy is
290 selective for fibers with low spontaneous rates. *J Neurophysiol* 110: 577-586.
291 14
292
293 15 Gillis KD (2000) Admittance-based measurement of membrane capacitance using the EPC-9
294 patch-clamp amplifier. *Pflugers Arch* 439: 655-664.
295 16
296
297 17 Glowatzki E, Fuchs PA (2002) Transmitter release at the hair cell ribbon synapse. *Nat*
298 *Neurosci* 5: 147-154.
299 18
300
301 19 Goutman JD, Glowatzki E (2007) Time course and calcium dependence of transmitter release
302 at a single ribbon synapse. *Proc Natl Acad Sci USA* 104: 16341-16346.
303 20
304
305 21 Goutman J, Glowatzki E (2011) Short-term facilitation modulates size and timing of the
306 synaptic response at the inner hair cell ribbon synapse. *J Neurosci* 31: 7974-7981.
307 22
308
309 23 Goutman JD (2012) Transmitter release from cochlear hair cells is phase locked to cyclic
310 stimuli of different intensities and frequencies. *J Neurosci* 32: 17025-17035.
311 24
312
313 25 Graydon CW, Cho S, Li GL, Kachar B, von Gersdorff H (2011) Sharp Ca^{2+} nanodomains
314 beneath the ribbon promote highly synchronous multivesicular release at hair cell
315 synapses. *J Neurosci* 31: 16637–16650.
316 26
317
318 27
319 28 Graydon CW, Cho S, Diamond JS, Kachar B, von Gersdorff H, Grimes WN (2014)
320 Specialized postsynaptic morphology enhances neurotransmitter dilution and high-
321 frequency signaling at an auditory synapse. *J Neurosci* 34: 8358-8372.
322 29
323 30
324
325 31 Greenwood DD (1990) A cochlear frequency-position function for several species-29 years
326 later. *J Acoust Soc Am* 87: 2592-2605.
327 32
328
329 33 Grothe B, Pecka M, McAlpine D (2010) Mechanisms of sound localization in mammals.
330 *Physiol Rev* 90: 983-1012.
331 34

- 332
333
- 334 1 Hackney CM, Mahendrasingam S, Jones EM, Fettiplace R (2003) The distribution of calcium
335 2 buffering proteins in the turtle cochlea. *J Neurosci* 23: 4577-4589.
- 336
337
- 338 3 Hackney CM, Mahendrasingam S, Penn A, Fettiplace R (2005) The concentrations of calcium
339 4 buffering proteins mammalian cochlear hair cells. *J Neurosci* 25: 7867-7886.
- 340
341
- 342 5 Heil P, Peterson AJ (2017) Spike timing in auditory-nerve fibers during spontaneous activity
343 6 and phase locking. *Synapse* 71: 5-36.
- 344
345
- 346 7 Heller S, Bell AM, Denis CS, Choe Y, Hudspeth AJ (2002) Parvalbumin 3 is an abundant
347 8 Ca^{2+} buffer in hair cells. *J Assoc Res Otolaryngol* 3: 488-498.
- 348
349
- 350 9 Johnson SL, Marcotti W, Kros CJ (2005) Increase in efficiency and reduction in Ca^{2+}
351 10 dependence of exocytosis during development of mouse inner hair cells. *J Physiol* 563:
352 11 177-191.
- 353
354
355
- 356 12 Johnson SL, Adelman JP, Marcotti W (2007) Disruption of spontaneous action potential
357 13 activity in inner hair cells of SK2 knockout mice prevents the normal development of
358 14 exocytotic machinery. *J Physiol* 583: 631-646.
- 359
360
361
- 362 15 Johnson SL, Marcotti W (2008) Biophysical properties of $\text{Ca}_v1.3$ calcium channels in gerbil
363 16 inner hair cells. *J Physiol* 586: 1029-1042.
- 364
365
- 366 17 Johnson SL, Forge A, Knipper M, Münkner S, Marcotti W (2008) Tonotopic variation in the
367 18 calcium dependence of neurotransmitter release and vesicle pool replenishment at
368 19 mammalian auditory ribbon synapses. *J Neurosci* 28: 7670-7678.
- 369
370
371
- 372 20 Johnson SL, Franz C, Knipper M, Marcotti W (2009) Functional maturation of the exocytotic
373 21 machinery at gerbil hair cell ribbon synapses. *J Physiol* 587: 1715-1726.
- 374
375
- 376 22 Johnson SL, Franz C, Kuhn S, Furness DN, Rüttiger L, Munkner S, Rivolta MN, Seward EP,
377 23 Herschman HR, Engel J, Knipper M, Marcotti W (2010) Synaptotagmin IV determines
378 24 the linear Ca^{2+} dependence of vesicle fusion at auditory ribbon synapses. *Nat Neurosci*
379 25 13: 45-52.
- 380
381
- 382 26 Johnson SL, Beurg M, Marcotti W, Fettiplace R (2011) Prestin-driven cochlear amplification
383 27 is not limited by the outer hair cell membrane time constant. *Neuron* 70: 1143-1154.
- 384
385
- 386 28 Johnson SL, Kennedy H, Holley MC, Fettiplace R, Marcotti W (2012) The resting transducer
387 29 current drives spontaneous activity in prehearing mammalian cochlear inner hair cells. *J*
388 30 *Neurosci* 32, 10479-10483.
- 389
390
391
- 392 31 Johnson SL (2015) Membrane properties specialize mammalian inner hair cells for frequency
393 32 or intensity encoding. *Elife* 4: e08177.
- 394
395
- 396 33 Keen EC, Hudspeth AJ (2006) Transfer characteristics of the hair cell's afferent synapse. *Proc*
397 34 *Natl Acad Sci USA* 103: 5537-5542.
- 398
399
400

- 401
402
403 1 Kros CJ, Ruppersberg JP, Rüsch A (1998) Expression of a potassium current in inner hair
404 2 cells during development of hearing in mice. *Nature* 394: 281-284.
405
406
407 3 Kujawa SG, Liberman MC (2009) Adding insult to injury: cochlear nerve degeneration after
408 4 "temporary" noise-induced hearing loss. *J Neurosci* 29: 14077-14085.
409
410
411 5 Kujawa SG, Liberman MC (2015) Synaptopathy in the noise-exposed and aging cochlea:
412 6 Primary neural degeneration in acquired sensorineural hearing loss. *Hear Res* 330: 191-
413 7 199.
414
415
416
417 8 Leão RM, von Gersdorff H (2009) Synaptic vesicle pool size, release probability and synaptic
418 9 depression are sensitive to Ca^{2+} buffering capacity in the developing rat calyx of Held.
419
420
421 10 *Braz J Med Biol Res* 42: 94-104.
422
423 11 Lenzi D, Runyeon JW, Crum J, Ellisman MK, Roberts WM (1999) Synaptic vesicle
424 12 populations in saccular hair cells reconstructed by electron tomography. *J Neurosci* 19:
425
426
427 13 119-132.
428
429 14 Lewis E, Leverenz E, Koyama H (1982) The tonotopic organization of the bullfrog amphibian
430 15 papilla, an auditory organ lacking a basilar membrane. *J Comp Physiol A Neuroethol*
431
432
433 16 *Sens Neural Behav Physiol* 145: 437-445.
434
435 17 Li G-L, Keen E, Andor-Ardó D, Hudspeth AJ, von Gersdorff H (2009) The unitary event
436 18 underlying multiquantal EPSCs at a hair cell's ribbon synapse. *J Neurosci* 29: 7558-
437
438
439 19 7568.
440
441 20 Li G-L, Cho S, von Gersdorff H (2014) Phase-locking precision is enhanced by multiquantal
442 21 release at an auditory hair cell ribbon synapse. *Neuron* 83: 1404-1417.
443
444
445 22 Lindau M, Neher E (1988) Patch-clamp techniques for time-resolved capacitance
446 23 measurements in single cells. *Pflugers Arch* 411: 137-146.
447
448
449 24 Magistretti J, Spaiardi P, Johnson SL, Masetto S (2015) Elementary properties of Ca^{2+}
450 25 channels and their influence on multivesicular release and phase-locking at auditory hair
451
452
453 26 cell ribbon synapses. *Front Cell Neurosci* 9: 123.
454
455 27 Marcotti W, Johnson SL, Holley MC, Kros CJ (2003) Developmental changes in the
456 28 expression of potassium currents of embryonic, neonatal and mature mouse inner hair
457
458
459 29 cells. *J Physiol* 548: 383-400.
460
461 30 Matthews G, Fuchs PA (2010) The diverse roles of ribbon synapses in sensory
462 31 neurotransmission. *Nat Rev Neurosci* 11: 812-822.
463
464
465 32 Meinrenken CJ, Borst JG, Sakmann B (2002) Calcium secretion coupling at calyx of held
466 33 governed by nonuniform channel-vesicle topography. *J Neurosci* 22: 1648-1667.
467

- 468
469
470 1 Meyer AC, Frank T, Khimich D, Hoch G, Riedel D, Chapochnikov NM, Yarin YM, Harke B,
471 2 Hell SW, Egner A, Moser T (2009) Tuning of synapse number, structure and function in
472 3 the cochlea. *Nat Neurosci* 12: 444–453.
473
474 4 Moser T, Beutner D (2000) Kinetics of exocytosis and endocytosis at the cochlear inner hair
475 5 cell afferent synapse of the mouse. *Proc Natl Acad Sci USA* 97: 883-888.
476
477 6 Müller M (1996) The cochlear place-frequency map of the adult and developing Mongolian
478 7 gerbil. *Hear Res* 94: 148-156.
479
480 8 Nakamura Y, Harada H, Kamasawa N, Matsui K, Rothman JS, Shigemoto R, Silver RA,
481 9 DiGregorio DA, Takahashi T (2015) Nanoscale distribution of presynaptic Ca^{2+}
482 10 channels and its impact on vesicular release during development. *Neuron* 85: 145-158.
483
484 11 Naraghi M, Neher E (1997) Linearized buffered Ca^{2+} diffusion in microdomains and its
485 12 implications for calculation of $[\text{Ca}^{2+}]$ at the mouth of a calcium channel. *J Neurosci* 17:
486 13 6961-6973.
487
488 14 Neher E (1998) Vesicle pools and Ca^{2+} microdomains: new tools for understanding their roles
489 15 in neurotransmitter release. *Neuron* 20: 389-399.
490
491 16 Nouvian R (2007) Temperature enhances exocytosis efficiency at the mouse inner hair cell
492 17 ribbon synapse. *J Physiol* 584: 535-542.
493
494 18 Palmer AR, Russell IJ (1986) Phase-locking in the cochlear nerve of the guinea-pig and its
495 19 relation to the receptor potential of inner hair-cells. *Hear Res* 24: 1-15.
496
497 20 Palmer MJ, Hull C, Vigh J, von Gersdorff H (2003) Synaptic cleft acidification and
498 21 modulation of short-term depression by exocytosed protons in retinal bipolar cells. *J*
499 22 *Neurosci* 23: 11332-11341.
500
501 23 Pangršič T, Gabrielaitis M, Michanski S, Schwaller B, Wolf F, Strenzke N, Moser T (2015)
502 24 EF-hand protein Ca_2^+ buffers regulate Ca_2^+ influx and exocytosis in sensory hair cells.
503 25 *Proc Natl Acad Sci USA* 112: E1028-1037.
504
505 26 Patel SH, Salvi JD, Ó Maoiléidigh D, Hudspeth AJ (2012) Frequency-selective exocytosis by
506 27 ribbon synapses of hair cells in the bullfrog's amphibian papilla. *J Neurosci* 32: 13433-
507 28 13438.
508
509 29 Pitchford S, Ashmore JF (1987) An electrical resonance in hair cells of the amphibian papilla
510 30 of the frog *Rana temporaria*. *Hear Res* 27: 75-83.
511
512 31 Platzter J, Engel J, Schrott-Fischer A, Stephan K, Bova S, Chen H, Zheng H, Striessnig J
513 32 (2000) Congenital deafness and sinoatrial node dysfunction in mice lacking class D L-
514 33 type Ca^{2+} channels. *Cell* 102: 89-97.
515
516
517
518
519
520
521
522
523
524
525
526
527
528
529
530
531
532
533
534

- 535
536
537 1 Roberts WM, Jacobs RA, Hudspeth AJ (1990) Colocalization of ion channels involved in
538 2 frequency selectivity and synaptic transmission at presynaptic active zones of hair cells.
539 3 J Neurosci 10: 3664-3684.
540 4
541 5 Rose JE, Brugge JF, Anderson DJ, Hind JE (1967) Phase-locked response to low-frequency
542 6 tones in single auditory nerve fibers of the squirrel monkey. J Neurophysiol 30: 769–
543 7 793.
544 8
545 9 Roux I, Safieddine S, Nouvian R, Grati M, Simmler MC, Bahloul A, Perfettini I, Le Gall M,
546 10 Rostaing P, Hamard G, Triller A, Avan P, Moser T, Petit C (2006) Otoferlin, defective
547 11 in a human deafness form, is essential for exocytosis at the auditory ribbon synapse.
548 12 Cell 127:277-289.
549 13 Russell IJ, Sellick PM (1978) Intracellular studies of hair cells in the mammalian cochlea. J
550 14 Physiol 284: 261-290.
551 15 Rutherford MA, Roberts WM (2006) Frequency selectivity of synaptic exocytosis in frog
552 16 saccular hair cells. Proc Natl Acad Sci USA 103: 2898–2903.
553 17 Safieddine S, El-Amraoui A, Petit C (2012) The auditory hair cell ribbon synapse: from
554 18 assembly to function. Ann Rev Neurosci 35: 509-528.
555 19
556 20 Schmidt H, Brachtendorf S, Arendt O, Hallermann S, Ishiyama S, Bornschein G, Gall D,
557 21 Schiffmann SN, Heckmann M, Eilers J (2013) Nanodomain coupling at an excitatory
558 22 cortical synapse. Curr Biol 23: 244-249.
559 23
560 24 Schnee ME, Lawton DM, Furness DN, Benke TA, Ricci AJ (2005) Auditory hair cell-afferent
561 25 fiber synapses are specialized to operate at their best frequencies. Neuron 47: 243-254.
562 26
563 27 Stanley EF (2016) The nanophysiology of fast transmitter release. Trends Neurosci 39: 183-
564 28 197.
565 29
566 30 Südhof TC (2002) Synaptotagmins: why so many? J Biol Chem 277: 7629–7632.
567 31
568 32 Van Hook MJ, Parmelee CM, Chen M, Cork KM, Curto C, Thoreson WB (2014) Calmodulin
569 33 enhances ribbon replenishment and shapes filtering of synaptic transmission by cone
570 34 photoreceptors. J Gen Physiol 144, 357-378.
571 35
572 36 Vincent PFY, Bouleau Y, Safieddine S, Petit C, Dulon D (2014) Exocytotic machineries of
573 37 vestibular type I and cochlear ribbon synapses display similar intrinsic otoferlin-
574 38 dependent Ca^{2+} sensitivity but a different coupling to Ca^{2+} channels. J Neurosci 34,
575 39 10853-10869.
576 40
577 41 Vyleta NP, Jonas P (2014) Loose coupling between Ca^{2+} channels and release sensors at a
578 42 plastic hippocampal synapse. Science 343, 665-670.
579 43
580
581
582
583
584
585
586
587
588
589
590
591
592
593
594
595
596
597
598
599
600
601

- 602
603
604 1 Wang LY, Augustine GJ (2015) Presynaptic nanodomains: a tale of two synapses. *Front Cell*
605 2 *Neurosci* 8: 455.
606
607
608 3 Wangemann P, Schacht J (1996) Homeostatic mechanisms in the cochlea. In: *The Cochlea*
609 4 (Dallos P, Popper A, Fay R, Eds.) 130–185 (Springer, New York).
610
611
612 5 Wong AB, Rutherford MA, Gabrielaitis M, Pangrsic T, Göttfert F, Frank T, Michanski S,
613 6 Hell S, Wolf F, Wichmann C, Moser T (2014) Developmental refinement of hair cell
614 7 synapses tightens the coupling of Ca²⁺ influx to exocytosis. *EMBO J* 33: 247-264.
615
616
617
618 8 Zampini V, Johnson SL, Franz C, Knipper M, Holley MC, Magistretti J, Masetto S, Marcotti
619 9 W (2013) Burst activity and ultrafast activation kinetics of Cav1.3 Ca²⁺ channels
620 10 support presynaptic activity in adult gerbil hair cell ribbon synapses. *J Physiol* 591:
621 11 3811-3820.
622
623
624 12 Zampini V, Johnson SL, Franz C, Lawrence ND, Münkner S, Engel J, Knipper M, Magistretti
625 13 J, Masetto S, Marcotti W (2010) Elementary properties of CaV1.3 Ca²⁺ channels
626 14 expressed in mouse cochlear inner hair cells. *J Physiol* 588: 187–199.
627
628
629
630
631
632 15

633
634
635
636
637
638
639
640
641
642
643
644
645
646
647
648
649
650
651
652
653
654
655
656
657
658
659
660
661
662
663
664
665
666
667
668
669
670
671
672
673
674
675
676
677
678
679
680
681
682
683

1 **Figure Legends**

2 **Figure 1. Ca^{2+} dependence of exocytosis in gerbil IHCs**

3 **A-C**, I_{Ca} and ΔC_m from apical (**A**: ~0.35 kHz), middle (**B**: ~2.5 kHz) and basal (**C**: ~30 kHz)
4 IHCs in the presence of 0.1 mM EGTA (left panel) and 10 mM EGTA (right panel).
5 Recordings were obtained in response to 50 ms voltage steps from the holding potential of
6 -81 mV to -11 mV. For clarity, only responses at -81 mV and -11 mV are shown. **D-F**,
7 Average peak $I-V$ and ΔC_m-V curves in apical (**D**: 0.1 mM EGTA, P20-P21, $n = 6$; 10 mM
8 EGTA, P21-P27, $n = 8$), middle (**E**: 0.1 mM EGTA, P23-P24, $n = 6$; 10 mM EGTA, P23-P24,
9 $n = 7$) and basal (**F**: 0.1 mM EGTA, P18-P27, $n = 13$; 10 mM EGTA, P21-P27, $n = 10$) IHCs.

10

11 **Figure 2. Kinetics of vesicle release in gerbil IHCs**

12 **A-C**, ΔC_m from apical (**A**), middle (**B**) and basal (**C**) IHCs in the presence of 0.1 mM EGTA
13 (black traces) and 10 mM EGTA (grey traces). Recordings were obtained in response to
14 voltage steps from 2 ms to 1.0 s (to around -11 mV) elicit both the RRP and SRP. For clarity,
15 only a few responses are shown. **D-F**, Average ΔC_m obtained using the above protocol from
16 apical (**D**: 0.1 mM EGTA, $n = 8$; 10 mM EGTA, $n = 3$), middle (**E**: 0.1 mM EGTA, $n = 5$; 10
17 mM EGTA, $n = 6$) and basal (**F**: 0.1 mM EGTA, P18-P20, $n = 6$; 10 mM EGTA, P21-P31, n
18 = 11) IHCs revealing the SRP. **G-I**, Isolated RRP (first 50 ms expanded from **D-F**)
19 approximated with single exponential functions from the average data (apical, **G**: 0.1 mM
20 EGTA, maximum $\Delta C_m = 19.2 \pm 5.0$ fF, $\tau = 31 \pm 12$ ms; 10 mM EGTA, $\Delta C_m = 11.1 \pm 1.0$ fF,
21 $\tau = 18 \pm 3$ ms; middle, **H**: 0.1 mM EGTA, $\Delta C_m = 19.9 \pm 5.8$ fF, $\tau = 25 \pm 13$ ms; 10 mM
22 EGTA, $\Delta C_m = 7.9 \pm 1.3$ fF, $\tau = 21 \pm 8$ ms; basal, **I**: 0.1 mM EGTA, $\Delta C_m = 23.1 \pm 5.7$ fF, $\tau =$
23 28 ± 12 ms; 10 mM EGTA, data could not be fitted because ΔC_m was almost absent.

24

25

684
685
686
687
688
689
690
691
692
693
694
695
696
697
698
699
700
701
702
703
704
705
706
707
708
709
710
711
712
713
714
715
716
717
718
719
720
721
722
723
724
725
726
727
728
729
730
731
732
733
734

1 **Figure 3. Kinetics of vesicle release in endogenous Ca^{2+} buffer from gerbil IHCs**

2 *A*, ΔC_m from apical (black) and basal (grey) IHCs recorded with perforated patch.
3 Recordings were obtained as described in **Fig. 2**. For clarity, only a few responses are shown.
4 *B*, Average ΔC_m from apical (P37-P52, $n = 4$) and basal (P37-P60, $n = 5$) IHCs revealing the
5 RRP and SRP. *C*, Isolated RRP (first 50 ms expanded from *B*) approximated with single
6 exponential functions from the single data (apical, maximum $\Delta C_m = 11.6 \pm 1.8$ fF, $\tau = 26 \pm 10$
7 ms; basal, $\Delta C_m = 12.2 \pm 3.2$ fF, $\tau = 31 \pm 17$ ms). *D*, The perforated-patch values of ΔC_m at 20
8 ms, a value that is well within the range of the RRP, were extrapolated (dotted lines) to those
9 obtained using different EGTA concentrations (data from **Fig. 2**). The 1 mM EGTA data are
10 from Johnson et al., 2008.

11
12 **Figure 4. Ca^{2+} currents and ΔC_m in mouse IHCs**

13 *A, B*, I_{Ca} (top panels) and ΔC_m (bottom panels) responses recorded from IHCs positioned in
14 the apical region (CF: ~ 3.0 kHz) of the mouse cochlea in the presence of low (0.1 & 1 mM)
15 and high (10 mM) concentrations of intracellular EGTA, respectively. Recordings were
16 obtained in response to 50 ms voltage steps from the holding potential of -81 mV to -11 mV.
17 *C, D*, Average peak current-voltage (I - V , bottom panel) and capacitance-voltage (ΔC_m - V , top
18 panel) curves from IHCs recorded in the presence of low and high intracellular EGTA,
19 respectively. *E*, Average ΔC_m in response to voltage steps from 2 ms to 1.0 s (to around -11
20 mV) showing the RRP and SRP. *F*, RRP (first 50 ms expanded from panel *E*) approximated
21 with single exponential functions for the difference concentrations of EGTA used (0.1 & 1
22 mM: maximum $\Delta C_m = 16.4 \pm 3.4$ fF, $\tau = 32 \pm 10$ ms; 10 mM: $\Delta C_m = 3.4 \pm 0.4$ fF, $\tau = 17 \pm 2$
23 ms). The available RRP (see text) was calculated using a conversion factor of 37 aF/vesicle
24 (Lenzi et al., 1999).

735
736737 1 **Figure 5. Ca^{2+} currents and ΔC_m in bullfrog hair cells tuned to ~ 400-500 Hz sound**

738

739 2 **signals**

740

741 3 **A**, Calcium current (I_{Ca}) and membrane capacitance (C_m) were measured while hair cells were

742

743 4 depolarized from a holding potential of -90 mV to -30 mV for 20 ms (black), 100 ms (grey),

744

745 5 and 500 ms (light grey) with 0.1 mM (left), 2 mM (middle), and 10 mM of intracellular

746

747 6 EGTA (right). Note the change in vertical scales for the C_m data and the large ΔC_m jump

748

749 7 (exocytosis) produced by 500 ms depolarizing pulses when 0.1 mM EGTA is used in the

750

751 8 patch pipette internal solution. **B**, Average ΔC_m in response to voltage steps from 2 ms to 50

752

753 9 ms with 2 mM (black) and 10 mM EGTA (grey). The depolarization of 50 ms from -90 mV

754

755 10 to -30 mV only showed significant difference of ΔC_m between 2 mM and 10 mM EGTA

756

757 11 (asterisk, unpaired t-test, $p < 0.05$). Data modified from Graydon et al., 2011. **C**, Comparison

758

759 12 of ΔC_m in response to voltage steps of 20 ms from -90 mV to -30 mV using 0.1 mM (light

760

761 13 grey, $n = 27$, 21.7 ± 1.7 fF), 2 mM (black, $n = 18$, 17.8 ± 1.4 fF), and 10 mM (grey, $n = 14$,

762

763 14 17.4 ± 1.0 fF) of EGTA. ΔC_m was measured after 4 minutes since the break-in. One-way

764

765 15 ANOVA did not show significant difference ($p = 0.098$). **D**, Comparison of ΔC_m in response

766

767 16 to voltage steps of 500 ms pulse from -90 mV to -30 mV using 0.1 mM (light grey, $n = 16$,

768

769 17 203.8 ± 34.8 fF), 2 mM (black, $n = 34$, 147.3 ± 9.1 fF), and 10 mM (grey, $n = 13$, 104.1 ± 8.5

770

771 18 fF) of EGTA. The ΔC_m jump was measured after 4 minutes from whole-cell break-in to allow

772

773 19 for the full diffusion of EGTA into the hair cell. One-way ANOVA followed the Bonferroni

774

775 20 test that showed significant difference (overall: $p = 0.006$).

776

777 21

778

779 22 **Figure 6. Rate of ΔC_m recovery in gerbil IHCs.**

780

781 23 **A**, Schematic diagram of the paired-pulse protocol used to stimulate IHCs. ΔC_m was elicited

782

783 24 in response to 50 ms depolarizing voltage steps to -11 mV (holding potential of -81 mV) at

784

785 25 time 0 and varying the interpulse interval (IPI = 10 ms, 20 ms, 40 ms, 100ms 200 ms, 500 ms,

786
787
788
789
790
791
792
793
794
795
796
797
798
799
800
801
802
803
1804
805
808
809
810
811
812
813
814
815
816
817
818
819
820
821
822
823
824
825
826
827
828
829
830
831
832
833
834
835
836
837
838
839
840

1 1s) after the initial step. **B, C**, I_{Ca} and ΔC_m from apical (**B**: ~0.35 kHz) and basal (**C**: ~30 kHz)
2 IHCs in the presence of 0.1 mM EGTA (black) and 10 mM EGTA (grey). Voltage protocol is
3 as shown in panel **A**. **D, E**, Average ΔC_m ratio ($\Delta C_m^2/\Delta C_m^1$; see panel **A**) from apical (**D**) and
4 basal (**E**) IHCs. In apical IHCs (**D**), the data were plotted against IPI and fitted with a single
5 exponential function (0.1 mM EGTA, $\tau_1 = 42.1 \pm 8.1$ ms, $n = 12$; 10 mM EGTA, $\tau_1 = 75.1 \pm$
6 17.1 ms, $n = 6$; significantly different at $p < 0.0005$). Basal IHCs showed an initial facilitation
7 followed by a decline (**E**). In panel **E** the data from 10 mM EGTA were omitted because ΔC_m
8 was almost absent (see panel **C**), which made it difficult to measure $\Delta C_m^2/\Delta C_m^1$ ratio with
9 accuracy.

11 **Figure 7. Recovery from paired-pulse depression at bullfrog hair cell synapses is**
12 **significantly slower with 10 mM EGTA.**

13 **A, B**, EPSCs evoked by two depolarizing pulses were obtained by paired recordings from an
14 afferent fibre and an amphibian papilla bullfrog hair cell. The hair cell was depolarized from
15 -60 mV to -30 mV for 20 ms (black bars) with various interpulse intervals (20, 50, 200 and
16 500 ms). The intracellular Ca^{2+} buffer of the hair cells was 2 mM EGTA (**A**) or 10 mM EGTA
17 (**B**). Note that the first depolarizing pulse still evokes a large phasic EPSC (EPSC₁) when 10
18 mM EGTA is present in the hair cell. However, the recovery of the phasic component of the
19 second EPSC (EPSC₂) was significantly slower with 10 mM EGTA. **C**, Summary of the
20 paired pulse ratio (EPSC₂/EPSC₁) recovery time course. Two EPSCs were evoked by
21 depolarizing hair cells using a pair of 20 ms pulse with various interpulse intervals. 2 mM
22 (black, $n = 4-9$ pairs) and 10 mM EGTA (grey, $n = 5-8$) were used as intracellular calcium
23 buffers within hair cells. All the EPSCs were measured after 4 minutes from the whole-cell
24 break-in to allow for full dialysis with EGTA. Data with 2 mM EGTA were modified from
25 Cho et al., 2011. Paired-pulse ratio (PPR) with 20, 50, 100, 200 and 500 ms interpulse

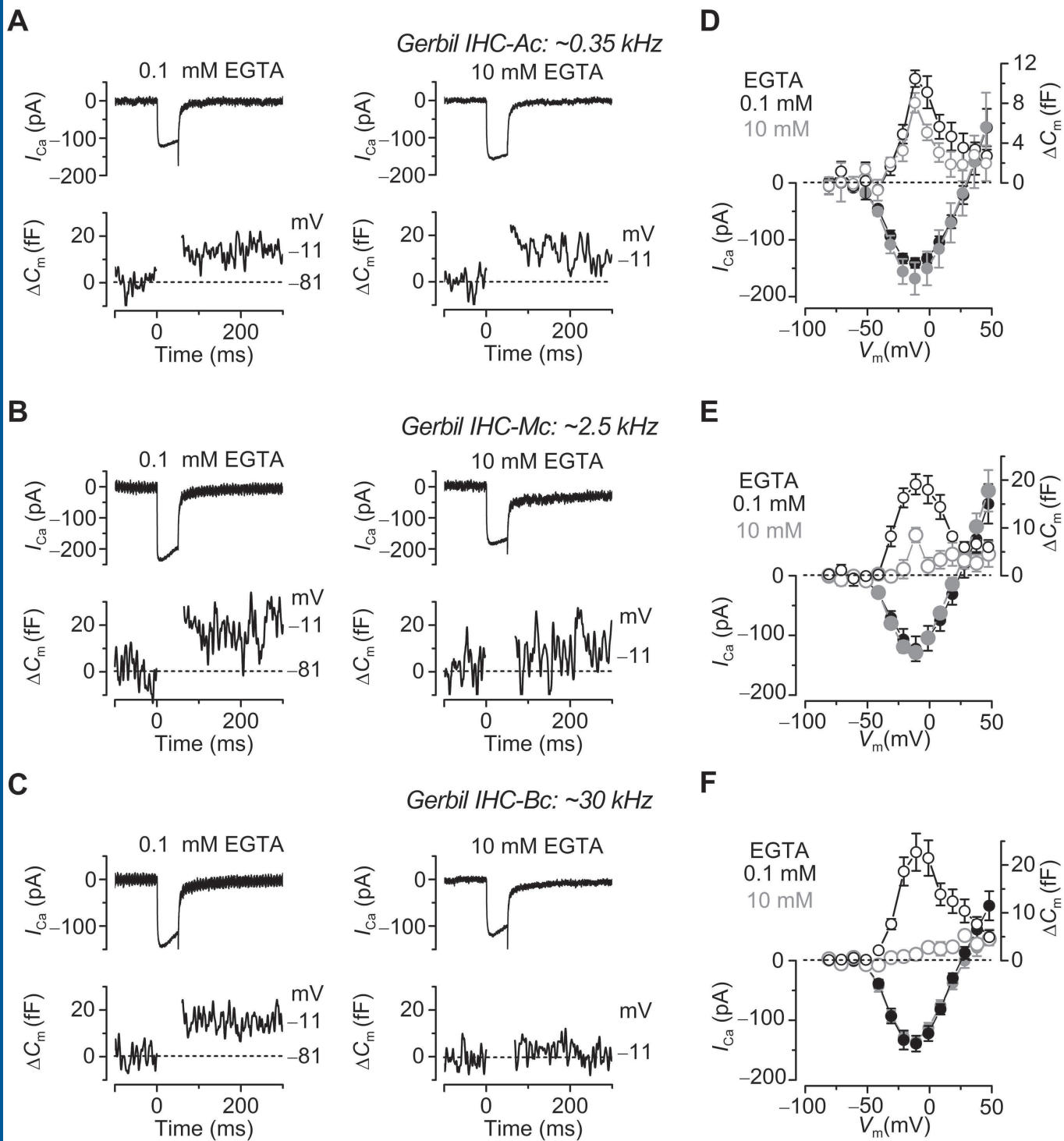
841
842
843
844
845
846
847
848
849
850
851
852
853
854
855
856
857
858
859
860
861
862
863
864
865
866
867
868
869
870
871
872
873
874
875
876
877
878
879
880

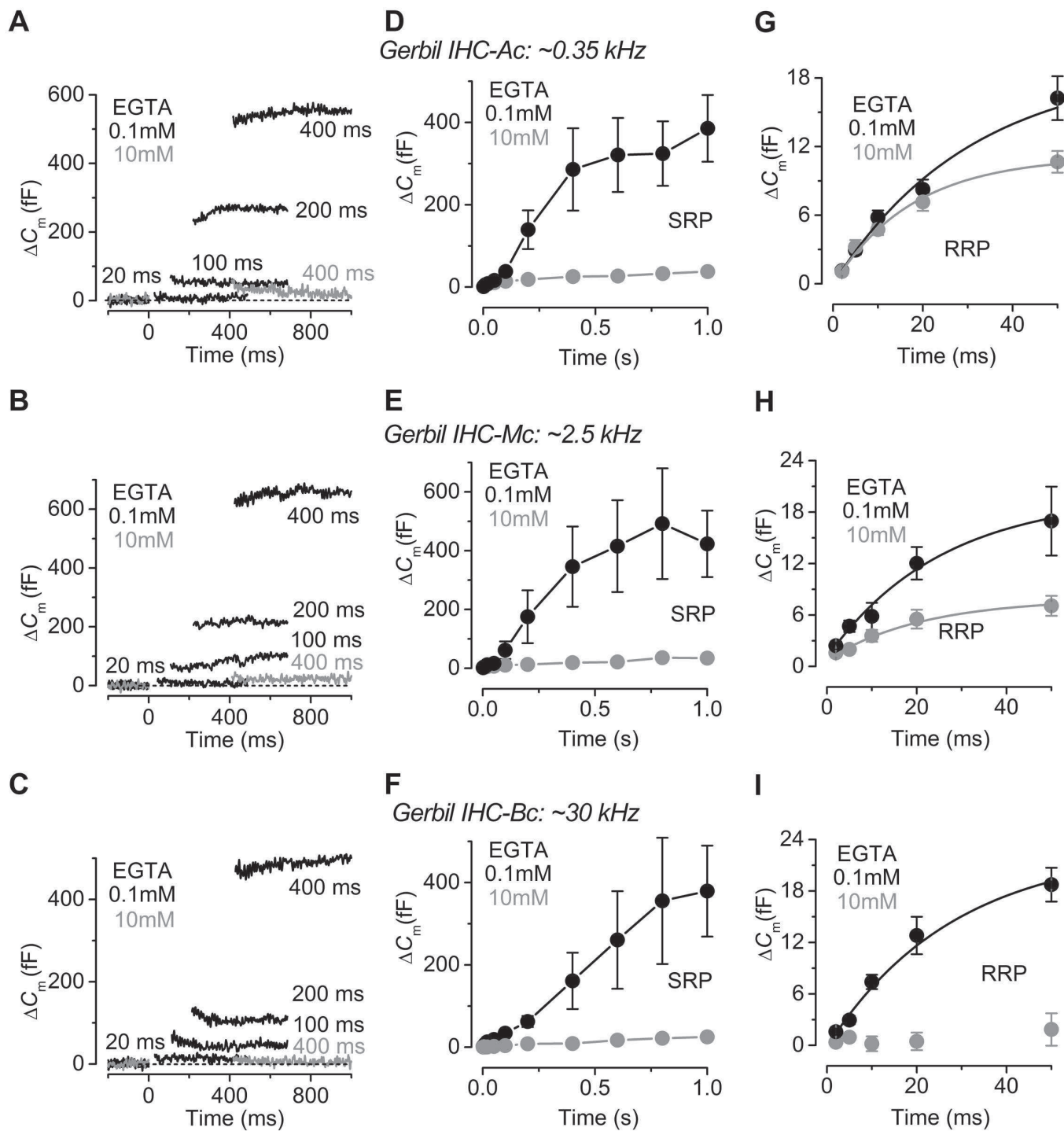
1 intervals were significantly different between 2 mM EGTA and 10 mM EGTA (* $p < 0.05$, **
2 $p < 0.01$, unpaired t-test).

3

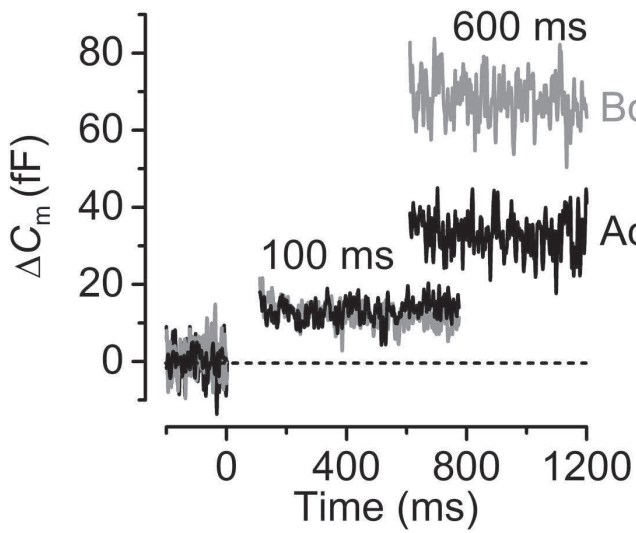
4 **Figure 8. Exocytosis in gerbil IHCs under *in vivo* resting membrane potential.**

5 **A, B**, I_{Ca} and ΔC_m from apical (**A**) and basal (**B**) IHCs in the presence of 1 mM EGTA in the
6 intracellular solution. Voltage protocol is as described in **Fig. 1** apart from the holding
7 membrane potential that was -51 mV for apical and -61 mV for basal IHCs. For clarity, only
8 responses at the resting membrane potential and the peak of I_{Ca} (-11 mV) are shown. **C, D**,
9 Average peak $I-V$ and ΔC_m-V curves in apical (**C**: P19-P28, $n = 7$) and basal (**D**: P19-P28, $n =$
10 9) IHCs. **E**, Average ΔC_m from apical (black: P19-P28, $n = 7$) and basal (grey: P19-P28, $n =$
11 5) IHCs obtained in response to voltage steps from 2 ms to 100 s (to -11 mV). Note that
12 voltage steps up to 50 ms could be fitted by a single exponential function, which reveals the
13 RRP, and values were: apical, maximum $\Delta C_m = 40.1 \pm 14.9$ fF, $\tau = 81 \pm 38$ ms; basal, $\Delta C_m =$
14 25.6 ± 10.5 fF, $\tau = 86 \pm 42$ ms. Voltage step to 100 ms were able to additionally recruit the
15 SRP. **F**, Average ΔC_m ratio ($\Delta C_m^2/\Delta C_m^1$; see **Fig. 6A**) from apical (black) and basal (grey)
16 IHCs elicited in response to 50 ms depolarizing voltage steps to -11 mV (holding potential of
17 -51 mV for apical and -61 mV for basal IHCs) at time 0 and varying the interpulse interval
18 (IPI) between 10 ms and 1s after the initial step. Data were well fitted with a single
19 exponential function.

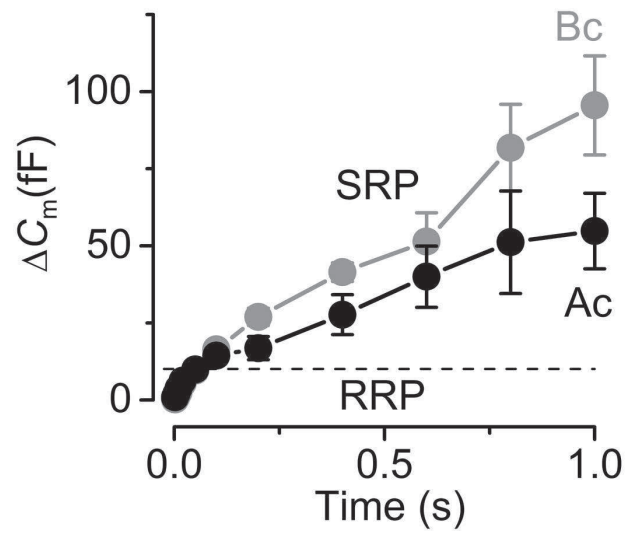




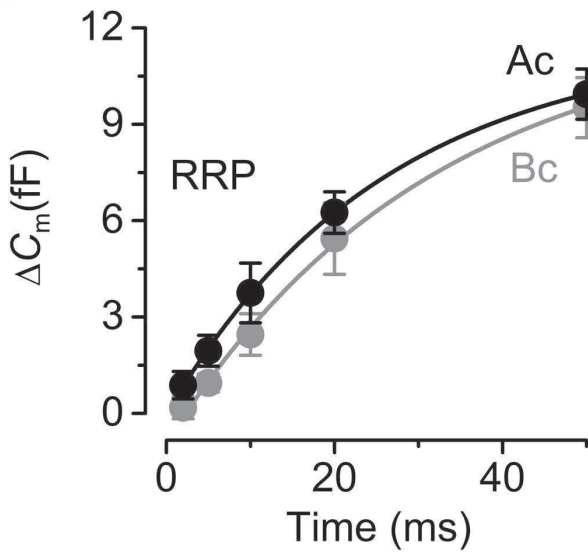
A



B



C



D

